AFRL-AFOSR-UK-TR-2022-0020

A conceptual and technical design study of a ultra-short pulse CO2 laser driven laser wakefield accelerator, as a first step to developing a robust demonstrator

Jaroszynski, Dino
UNIVERSITY OF STRATHCLYDE VIZ ROYAL COLLEGE OF SCIENCE & TECHNOLOGY
16 RICHMOND STREET
50 RICHMOND ST
GLASGOW, LANARKSHIRE, G1 1XT
GBR

01/26/2022
Final Technical Report

Air Force Research Laboratory
Air Force Office of Scientific Research
European Office of Aerospace Research and Development
Unit 4515 Box 14, APO AE 09421

REPORT DOCUMENTATION PAGE

PLEASE DO NOT RETURN YOUR FORM TO THE ABOVE ORGANIZATION.

1. REPORT DATE	2. REPORT TYPE	3. DATES COVERED	
		START DATE	END DATE
20220126	Final	20190915	20210914

4. TITLE AND SUBTITLE
A conceptual and technical design study of a ultra-short pulse CO2 laser driven laser wakefield accelerator, as a first step to developing a robust demonstrator

5a. CONTRACT NUMBER	5b. GRANT NUMBER	5c. PROGRAM ELEMENT NUMBER
	FA9550-19-1-7046	61102F
5d. PROJECT NUMBER	**5e. TASK NUMBER**	**5f. WORK UNIT NUMBER**

6. AUTHOR(S)
Dino Jaroszynski

7. PERFORMING ORGANIZATION NAME(S) AND ADDRESS(ES)
UNIVERSITY OF STRATHCLYDE VIZ ROYAL COLLEGE OF SCIENCE & TECHNOLOGY
16 RICHMOND STREET
50 RICHMOND ST
GLASGOW, LANARKSHIRE G1 1XT
GBR

8. PERFORMING ORGANIZATION REPORT NUMBER

9. SPONSORING/MONITORING AGENCY NAME(S) AND ADDRESS(ES)	10. SPONSOR/MONITOR'S ACRONYM(S)	11. SPONSOR/MONITOR'S REPORT NUMBER(S)
EOARD UNIT 4515 APO AE 09421-4515	AFRL/AFOSR IOE	AFRL-AFOSR-UK-TR-2022-0020

12. DISTRIBUTION/AVAILABILITY STATEMENT
A Distribution Unlimited: PB Public Release

13. SUPPLEMENTARY NOTES

14. ABSTRACT
Three major activates were undertaken for the project: i) design of a laser wakefield accelerator (LWFA) based on a CO2 laser, ii) design of an optically pumped CO2 ultra-short pulsed laser based on direct and indirect pumping, and iii) determine the cost of building an optically pumped CO2 laser prototype and a potential commercial device. This is described in a detailed report that is submitted as part of the overall report. The design studies of the LWFA and opti-cally pumped CO2 laser were undertaken in parallel. The CO2 laser driven LWFA design stud-ies were carried out at the University of Strathclyde, benefitting from an ongoing research pro-gramme to develop Ti:sapphire-pumped LWFAs and radiation sources at the University. The design study of the optically pumped CO2 laser was undertaken by IRP Technology LLC, Cor-rales, NM, USA as a sub-contract. The main people involved in the project were Prof. Dino Jaroszynski and Dr. Enrico Brunetti from Strathclyde, and Dr. Neil Campbell and Mr. Jack Lovell from IRP. Many other people from Strathclyde contributed to the work both directly and indirectly.
If the laser energy is increased to 100 J (P = 200 Tera-Watt), the spot size to 100 µm, and the plasma length is set to 20 mm, the mean energy of the selection is 560 Mega electron Volts (MeV) with 7% energy spread, 50 nano-coulombs (nC) charge and 15 milli-radian (mrad) r.m.s. divergence. If the laser energy is further increased to 400 J (P = 800 TW), with w0 = 200 µm, ne = 2.5 × 1016 cmâˆ'3 and a plasma length of 86 mm, the mean energy of the selection is 1.6 GeV with 12% energy spread, 140 nC charge and 6 mrad r.m.s. divergence. The electron bunch energy is 224 J, which results in a conversion efficiency of approximately 56%.

15. SUBJECT TERMS

16. SECURITY CLASSIFICATION OF:			17. LIMITATION OF ABSTRACT	18. NUMBER OF PAGES
a. REPORT	b. ABSTRACT	c. THIS PAGE		
U	U	U	SAR	7

19a. NAME OF RESPONSIBLE PERSON	19b. PHONE NUMBER *(Include area code)*
NATHANIEL LOCKWOOD	314-235-6005

A conceptual and technical design study of a ultra-short pulse CO_2 laser driven laser wakefield accelerator, as a first step to developing a robust demonstrator

Final report

D.A. Jaroszynski, E. Brunetti
SUPA, Department of Physics, University of Strathclyde, Glasgow, UK
R.N. Campbell, J. Lovell
IRP Technology LLC, Corrales, NM, USA

December 13, 2021

Introduction

Laser-wakefield accelerators (LWFAs) are compact devices capable of accelerating electrons to 100s MeV to GeV energies in mm to cm distances by exploiting the large electrostatic fields generated when an intense laser pulse propagates in underdense plasma. [1, 2]. This project aims to undertake a design study of a laser-wakefield accelerator driven by a mid-infrared CO_2 laser. A wavelength much longer than $0.8\,\mu m$ is chosen because the plasma response is driven by the ponderomotive force [3], which has a strength proportional to the square of the laser wavelength. This should result in more efficient LWFAs capable of producing electron beams with higher charge and narrower energy spread [4]. Furthermore, it has been shown that CO_2 lasers can be made very compact and efficient by optical pumping the gas medium of the laser [5], which makes it an excellent candidate for a robust compact system. The project is split into two chapters. The first chapter presents results of particle-in-cell (PIC) simulations performed at the University of Strathclyde to investigate the LWFA. The second chapter describes an initial conceptual design of an optically pumped CO_2 laser developed by IRP Technology.

LWFA driven by a CO_2 laser

Most laser-wakefield accelerators (LWFAs) demonstrated so far are driven by Ti:sapphire lasers operating at a typical wavelength of 0.8 µm and producing pulses with energy between 1 J and 50 J, duration between 1 fs and 100 fs, and repetition rate close to 1 Hz. After interaction with plasma, electron beams are generated with typical energy of 1–1000 MeV, divergence of 1–5 mrad, charge of 1–100 pC, normalised emittance of 1 π mm mrad or better and femtosecond pulse duration [6, 7, 8]. Over the last two decades significant advances have been achieved in the development of LWFA [9, 10, 11, 12]. Recently, quasimonoenergetic electrons with energy of 7.8 GeV and charge of 5 pC have been produced using an 850 TW laser system and a 20 cm long plasma with density of 2×10^{17} cm^{-3} [13].

Here we present results of particle-in-cell (PIC) simulations to model the interaction of an intense sub-picosecond laser pulse with wavelength $\lambda_0 = 10.6$ µm and pre-ionised uniform plasma of varying length. We investigated a wide range of laser pulse durations, waist sizes and energies for selected plasma densities, obtaining electron beams with energy up to 2 GeV and charge up to 100s nC, which is three orders of magnitude higher than what is achievable using near-infrared lasers of similar power.

Particle-in-cell simulation results

Particle-in-cell (PIC) simulations have been performed using the quasi-3D code FBPIC [14] to model a LWFA driven by a short laser pulse with wavelength $\lambda_0 = 10.6$ µm interacting with a pre-ionised uniform plasma. The pulse is linearly polarised and has a temporal $\cos^2$ shape with duration between 125 fs and 1 ps (FWHM of the intensity). The transverse profile is Gaussian, focused to a waist size w_0 between 25 µm and 300 µm (in vacuum) at the entrance of a pre-ionised uniform plasma of varying length preceded by a 60 µm long up-ramp. Simulations have also been performed using a plasma with radial density profile $n_r = n_e + a\, r^2$, where a has been varied between 8×10^{28} m^{-5} and 1.5×10^{29} m^{-5}. This models a preformed plasma waveguide [15]. The number of azimuthal (θ) modes is 2 and the number of macro-particles per cell in longitudinal, radial and azimuthal direction is $n_z = 2$, $n_r = 2$ and $n_\theta = 8$, with cubic particle shape. The box size has been changed depending on the laser and plasma parameters. Typically, the length in the longitudinal direction z is 1–1.5 mm and the radius is 0.6–1 mm. The resolution is about 0.4–0.6 µm in the longitudinal direction and 0.6–1 µm in the radial direction. A few simulations have also been performed using a higher longitudinal resolution of 0.1 µm, observing no significant differences in the average values reported here. A few simulations

performed using 3 azimuthal modes also produced similar results, except for small differences in the bunch structure. Most simulations use a radial boundary with perfectly-matched-layers and 256–512 damping cells.

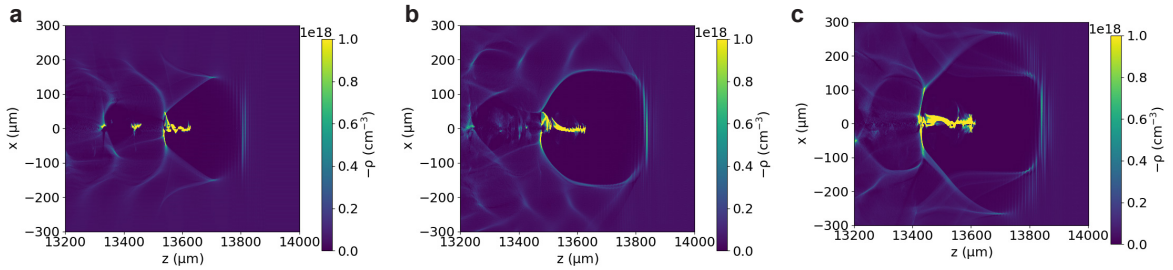

Figure 1: Electron density distribution created in a plasma with density of $5 \times 10^{16}\,\mathrm{cm}^{-3}$ by a laser pulse with a wavelength of 10.6 μm, normalised vector potential $a_0 = 5$, pulse duration of 500 fs (FWHM) and initial waist size of a) 100 μm b) 200 μm and c) 300 μm. The propagation distance is 14 mm.

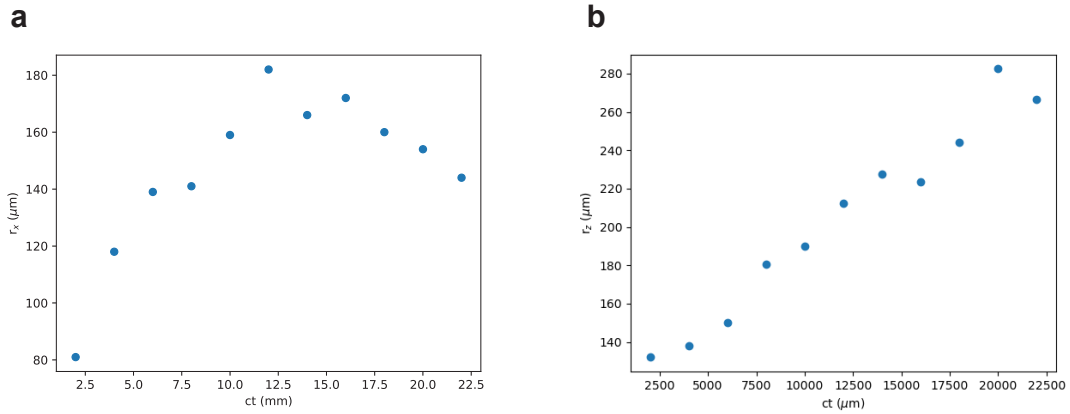

Figure 2: Bubble size versus propagation distance for a plasma with density of $1 \times 10^{17}\,\mathrm{cm}^{-3}$ and a laser pulse with a wavelength of 10.6 μm, energy of 100 J, pulse duration of 500 fs (FWHM) and waist size of 100 μm. a) Bubble size in the laser polarisation plane. b) Longitudinal bubble size.

Fig. 1 shows the accelerating structure created by a 500 fs duration (FWHM) laser pulse with normalised vector potential $a_0 = 5$ for three different waist sizes. The laser pulse propagates in a pre-ionised uniform plasma with density of $5 \times 10^{16}\,\mathrm{cm}^{-3}$. The ponderomotive force of the laser pulse pushes electrons away from the regions of high intensity, resulting in the formation of a cavity ("bubble" or "blowout") filled with ions and surrounded by a "sheath" of electrons. Background plasma electrons that are trapped inside the bubble are accelerated to relativistic energies by the strong electrostatic fields arising from charge separation. The bubble shape and size depends on the plasma density, on the laser power and on the strength of the fields of the electrons trapped inside (beam loading). These parameters usually vary during propagation, which leads to bubble evolution. A representative example is shown in Fig. 2 and a more

detailed discussion is provided below. Changes in bubble size can affect the injection rate and the accelerating gradient, resulting in the production of trains of bunches, or single bunches with a complex energy spectrum and usually significant sub-structure. Depending on the laser and plasma parameters, electrons injected late can form low-energy peaks or tails, or can be accelerated to high energies and account for most of the charge. Electrons injected early can form a low-charge high-energy wing, or can be decelerated back to low energies. Electrons can also be trapped inside cavities created further behind the laser pulse, but these are not considered here.

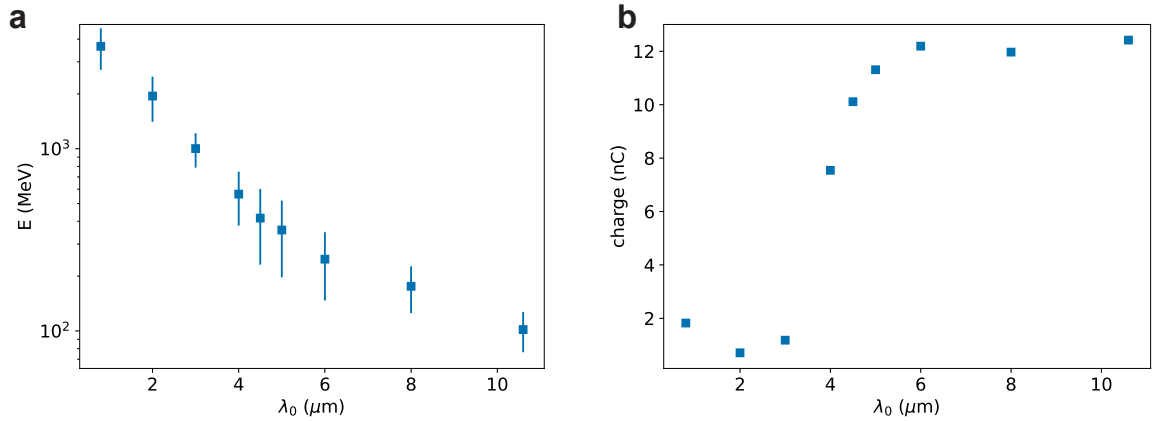

Figure 3: (a) Mean energy and (b) charge of electron beams produced by a laser pulse with duration of 250 fs (FWHM), waist size of 50 µm, normalised vector potential $a_0 = 5$ and varying wavelength after interaction with a pre-ionised plasma with density of 1×10^{17} cm^{-3}. The error bars represent the r.m.s. energy spread.

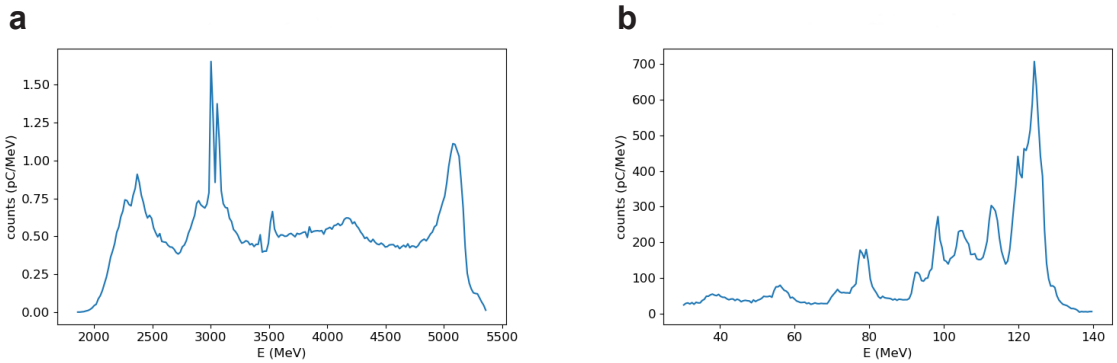

Figure 4: Electron beam spectrum produced in a pre-ionised plasma with density of 1×10^{17} cm^{-3} by a laser pulse with duration of 250 fs (FWHM), waist size of 50 µm, normalised vector potential $a_0 = 5$ and wavelength (a) 0.8 µm and (b) 10.6 µm.

The plasma response to the laser field is driven by the ponderomotive force, which depends on the wavelength. Its effect on the electron beam properties is shown in Fig. 3 for a laser pulse with a wavelength λ_0 between 0.8 µm and 10.6 µm. The pulse has duration $T_{FWHM} = 250$ fs, waist size $w_0 = 50$ µm and $a_0 = 5$, which corresponds to an energy of about 550 J (2 PW)

at 0.8 µm and 3.2 J (12 TW) at 10.6 µm. The plasma has a uniform profile with density of 1×10^{17} cm^{-3}. For $\lambda_0 = 0.8$ µm, the electron beam energy is about 3.6 GeV with 25% energy spread and a charge of 1.8 nC, after 200 mm propagation, which is slightly before dephasing. The laser-to-electron energy conversion efficiency is 1.2%. The normalised emittance is about $15\,\pi$ mm mrad, the r.m.s. divergence 1 mrad and the r.m.s. bunch length 6 µm. Electrons are injected into the bubble after about 10 mm and the corresponding acceleration gradient is about 20 GeV/m. The resulting energy spectrum is shown in Fig. 4a. When λ_0 is increased for fixed a_0, the laser energy decreases, resulting in a lower electron beam energy. The charge is also expected to decrease with laser energy, but this effect is counteracted by the stronger plasma response at longer wavelengths, resulting in a charge of about 12 nC for $\lambda_0 \gtrapprox 6$ µm. The bunch length also increases, whereas the transverse beam size remains close to 5 µm. For $\lambda_0 = 10.6$ µm, the electron beam mean energy is 100 MeV with 21% energy spread and a charge of 12 nC after 9 mm propagation. The laser energy to beam energy conversion efficiency is 40%, the normalised emittance $20\,\pi$ mm mrad, the r.m.s. divergence 20 mrad and the r.m.s. bunch length 50 µm. Injection into the bubble occurs after about 6 mm and the corresponding acceleration gradient is about 30 GeV/m. The resulting energy spectrum is shown in Fig. 4b. If the laser energy is kept constant at about 550 J ($a_0 = 66$), a CO_2 laser produces an electron beam with mean energy of 750 MeV, 65% energy spread and 530 nC charge in a 15 mm long plasma, corresponding to an efficiency of 70%. The normalised emittance is about $750\,\pi$ mm mrad, the r.m.s. divergence 75 mrad and the r.m.s. bunch length 170 µm. If only the high-energy peak is selected (1.25 GeV $< E <$ 1.45 GeV), the mean energy is 1.3 GeV with 3% energy spread, 130 nC charge and 10 mrad r.m.s. divergence.

These results suggest that a LWFA driven by a 10.6 µm laser can produce electron beams with significantly higher charge than currently possible using near-infrared lasers of the same power, although the electron energy is somewhat lower and the divergence, bunch length and emittance are larger. Near-infrared lasers have the advantage of supporting higher plasma densities, due to the higher critical density. This can help reduce the gap in charge. For example, a 0.8 µm, 2 PW laser delivering pulses with 35 fs duration and 75 J energy into a plasma with a density of 1.5×10^{19} cm^{-3} produces an electron beam with 860 MeV energy, 69% energy spread and 45 nC charge with an efficiency of 50%. For a high-energy selection (1 GeV $< E <$ 1.85 GeV), the mean energy is 1.4 GeV with 17% energy spread and 22 nC charge. Nevertheless, this is still 5 times lower than the charge predicted for a CO_2 laser with the same power.

Dependence on laser energy

In this section we investigate the performance of a LWFA operating at a wavelength of 10.6 µm for varying laser energy, fixed pulse duration, and selected waist sizes. The phase-space distribution of electrons accelerated inside the first bubble to an energy $E > 30$ MeV has been extracted when the mean energy is maximum, and properties such as the beam size, charge and energy spread have been calculated. These values describe the entire bunch, which can have a complex energy spectrum that is characterised by multiple peaks and long wings, but properties of selected quasi-monoenergetic peaks are also provided in the text.

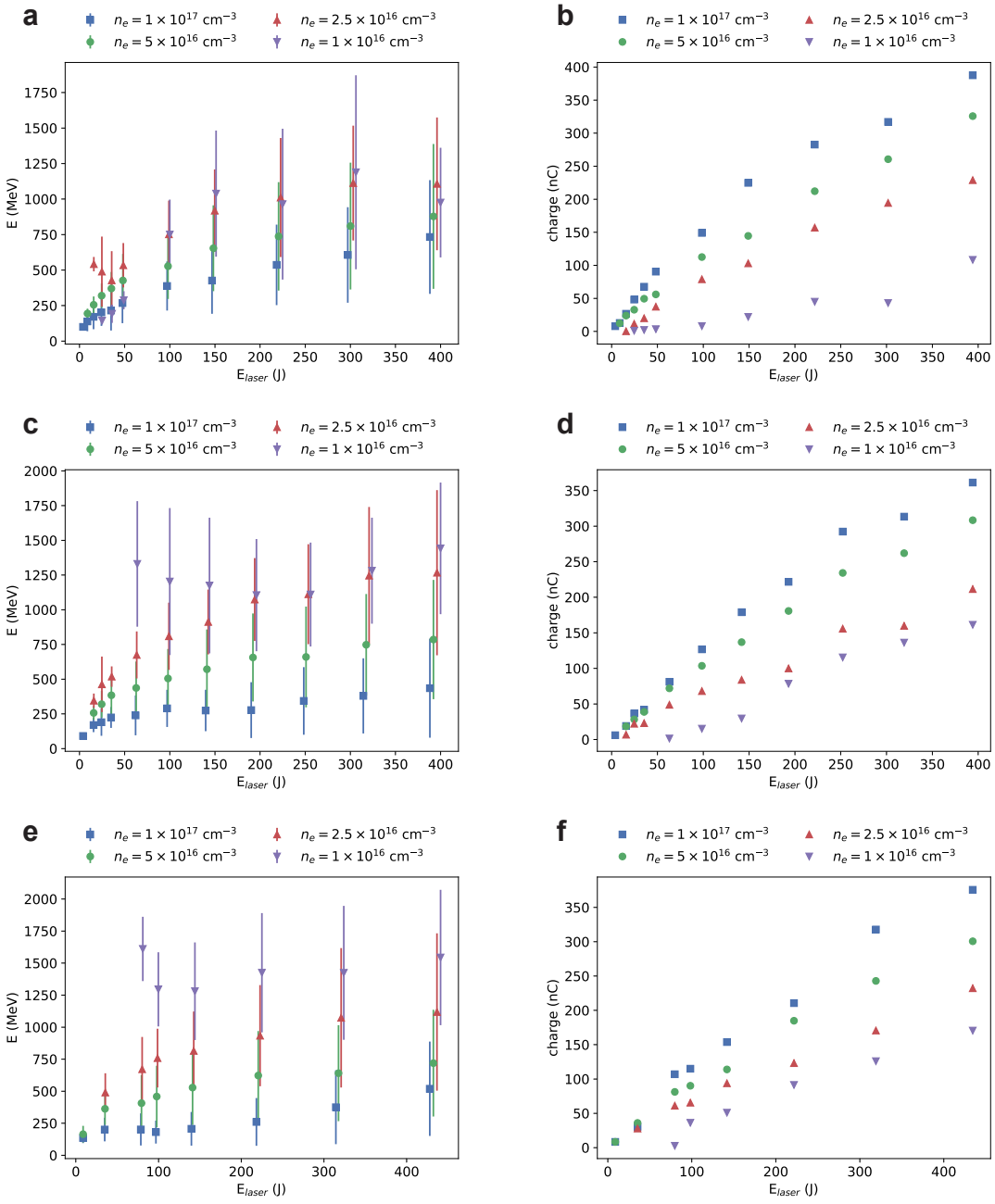

Figure 5: (a, c, e) Mean energy and (b, d, e) charge of electron beams produced in a pre-ionised plasma of varying density by a laser pulse with duration of 500 fs (FWHM), wavelength of 10.6 µm, while varying energy, and waist size of (a, b) 100 µm, (c, d) 200 µm and (e, f) 300 µm. Error bars correspond to the r.m.s. energy spread.

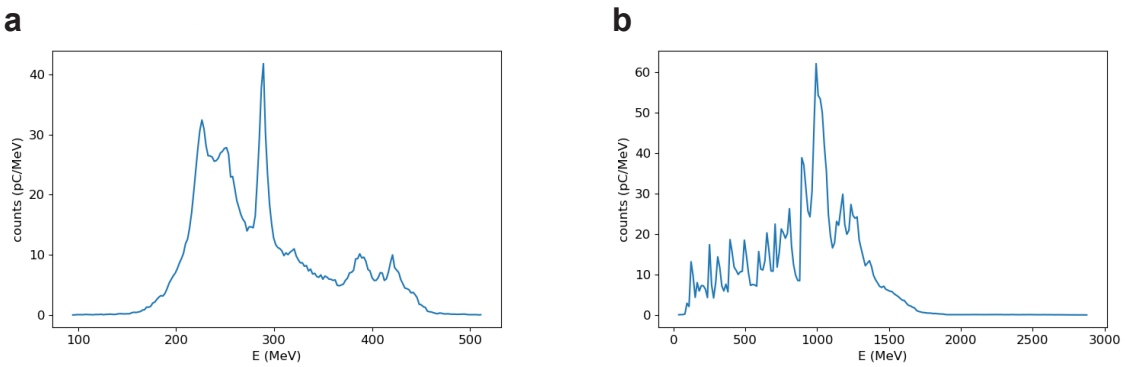

Figure 6: Electron beam spectrum produced in a pre-ionised plasma with density of $1 \times 10^{16}\,\mathrm{cm}^{-3}$ by a laser pulse with duration of 500 fs (FWHM), waist size of 100 µm, energy of 50 J ($a_0 = 7$) wavelength 0.8 µm in (a) a uniform plasma (b) a plasma with transverse parabolic profile defined by $a = 1.5 \times 10^{29}\,\mathrm{m}^{-5}$.

Fig. 5 shows the mean energy (a, c, e) and charge (b, d, f) of electron beams generated in a pre-ionised plasma with density between $1 \times 10^{16}\,\mathrm{cm}^{-3}$ and $1 \times 10^{17}\,\mathrm{cm}^{-3}$ by a laser pulse with 500 fs duration, energy between 2 J and 440 J (4–850 TW), and beam waist of 100 µm (a, b), 200 µm (b, c) and 300 µm (d, e). As the laser energy increases, electron beams with energy up to about 1.5 GeV and charge up to about 350 nC are obtained, observing similar trends for most plasma densities and laser waist sizes considered. The energy conversion efficiency is typically 10%–70%, also increasing with laser energy. Typically, the bunch length increases from about 10 µm to 150 µm, the divergence from 10 mrad to 50 mrad and the normalised emittance from $10\,\pi$ mm mrad to $1000\,\pi$ mm mrad. The acceleration length varies from about 10–20 mm for $n_e = 1 \times 10^{17}\,\mathrm{cm}^{-3}$ to 100–200 mm for $n_e = 1 \times 10^{16}\,\mathrm{cm}^{-3}$. In some cases, increasing the laser energy can result in late injection of a second bunch, which causes the mean electron energy to decrease. This is particularly evident for a plasma density of $1 \times 10^{16}\,\mathrm{cm}^{-3}$. A more detailed discussion of the scaling laws is provided in Section .

For a beam waist of 100 µm, the best operating plasma densities are $5 \times 10^{16}\,\mathrm{cm}^{-3}$ and higher. For plasma densities lower than $2.5 \times 10^{16}\,\mathrm{cm}^{-3}$ and low laser energies, self-focusing cannot balance diffraction and acceleration stops after relatively short distances. Background plasma electrons are also not fully evacuated from the accelerating structure, and the injected bunch drives an additional blowout, which degrades the beam quality. The resulting electron beam has a low energy and charge. For example, a laser pulse with an energy of 50 J ($a_0 = 7$) produces a 280 MeV electron beam with 3 nC charge in a plasma with a density of $1 \times 10^{16}\,\mathrm{cm}^{-3}$ and length of 47 mm (Fig. 6a). On the other hand, a laser pulse with the same parameters propagating in a plasma with parabolic radial profile produces an electron beam with an energy of 900 MeV and a charge of 25 nC in a length of 150 mm (Fig. 6b). However, for higher laser energies and larger waist sizes, electron beams with mean energy up to 1.5 GeV and 150 nC charge are obtained in a uniform plasma for this density and no significant differences are observed when using external guiding.

Electron energy spectra for selected laser and plasma parameters are presented in Fig. 7.

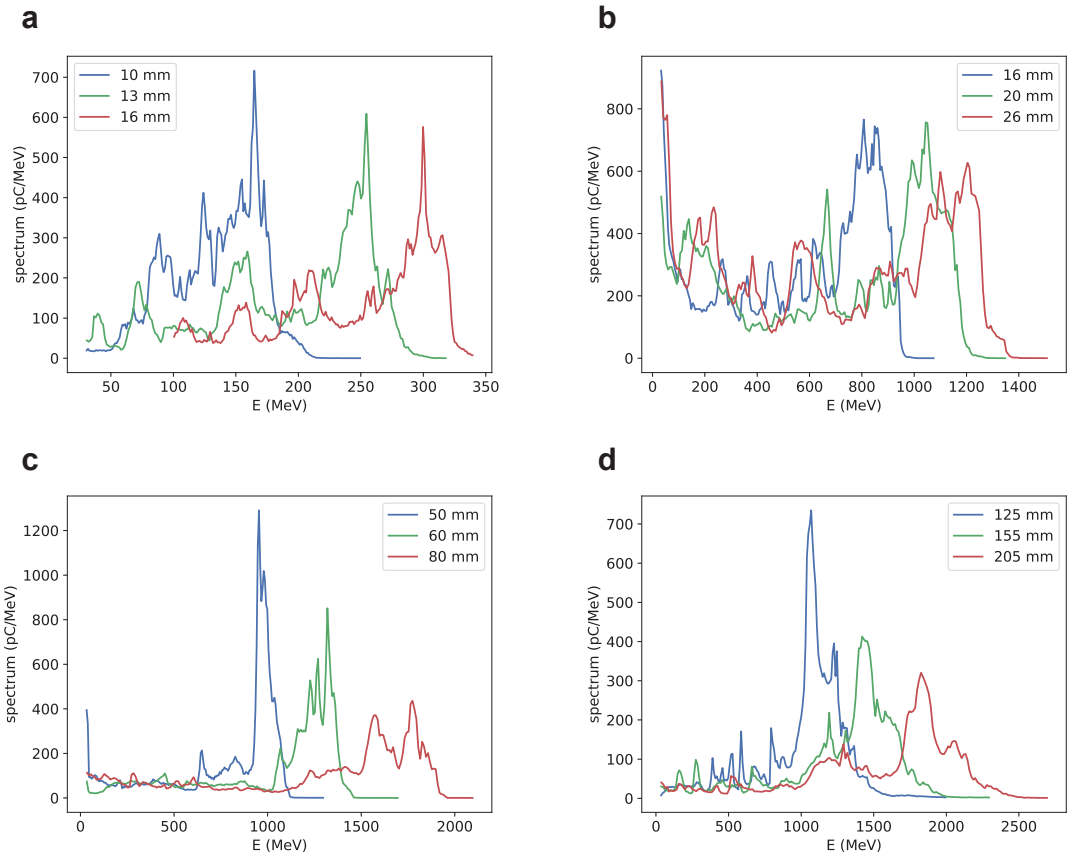

Figure 7: Selected electron energy spectra at different stages of acceleration produced in a pre-ionised plasma by a laser pulse with duration of 500 fs (FWHM) and wavelength of 10.6 µm. The laser waist size, normalised vector potential and plasma density are: a) $w_0 = 100\,\mu\text{m}$, $a_0 = 5$ ($E = 25\,\text{J}$), $n_e = 1 \times 10^{17}\,\text{cm}^{-3}$; b) $w_0 = 100\,\mu\text{m}$, $a_0 = 20$ ($E = 400\,\text{J}$), $n_e = 1 \times 10^{17}\,\text{cm}^{-3}$; c) $w_0 = 200\,\mu\text{m}$, $a_0 = 10$ ($E = 400\,\text{J}$), $n_e = 2.5 \times 10^{16}\,\text{cm}^{-3}$; d) $w_0 = 300\,\mu\text{m}$, $a_0 = 7$ ($E = 430\,\text{J}$), $n_e = 1 \times 10^{16}\,\text{cm}^{-3}$.

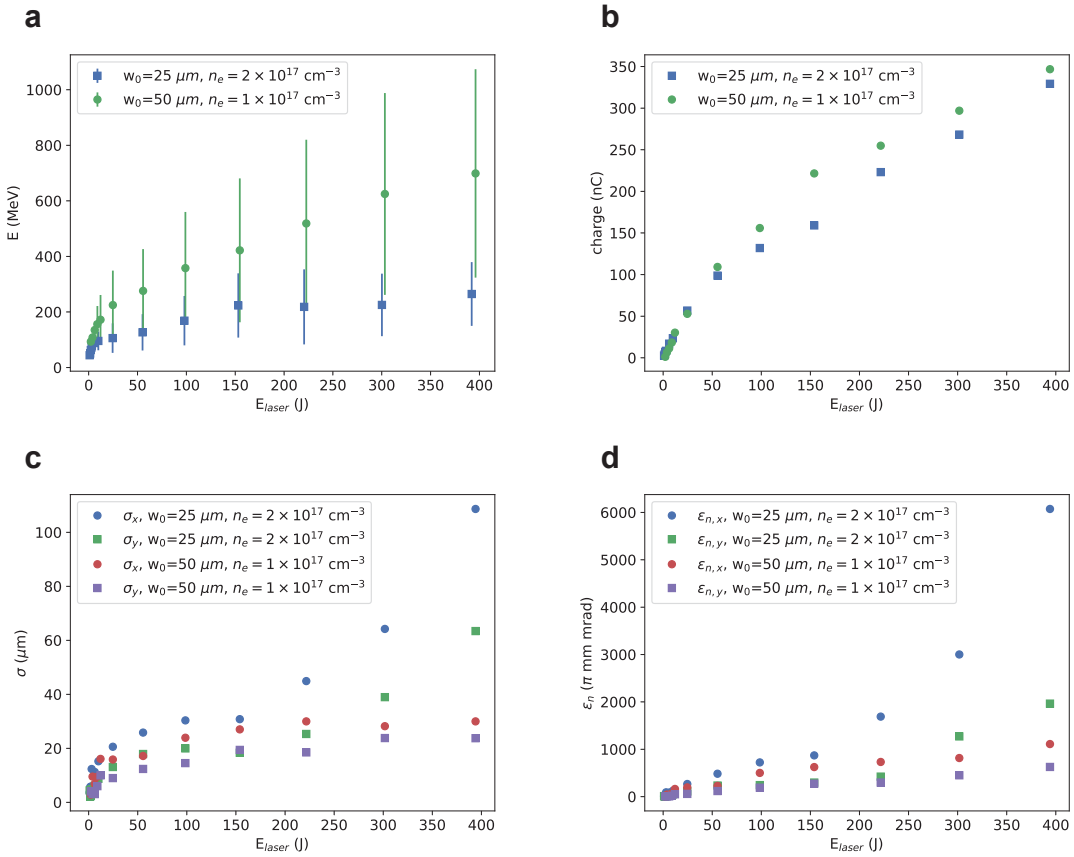

Figure 8: (a) Mean energy (b) charge (c) transverse size and (d) transverse normalised emittance of electron beams produced in a pre-ionised plasma of density 1×10^{17} cm^{-3} and 2×10^{17} cm^{-3} by a laser pulse with duration of 500 fs (FWHM), wavelength of 10.6 µm, varying energy, and waist size of 25 µm and 50 µm. Error bars correspond to the r.m.s. energy spread.

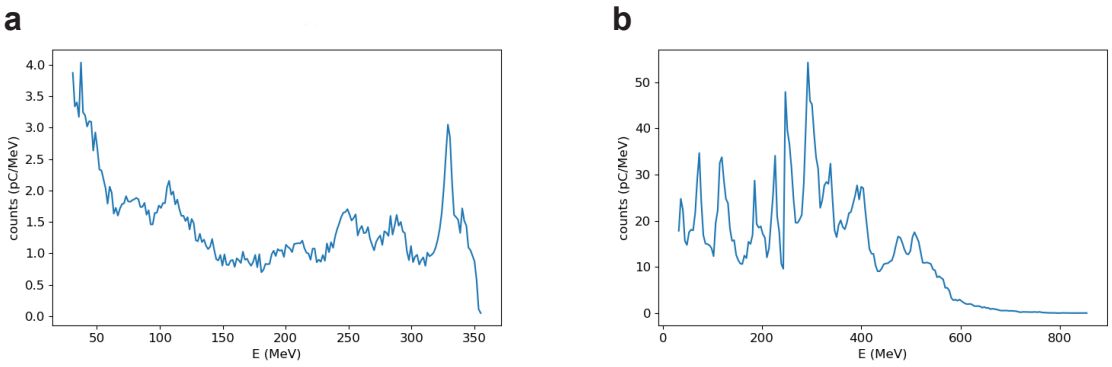

Figure 9: Electron beam spectrum produced in a pre-ionised plasma with density of 2.5×10^{16} cm^{-3} by a laser pulse with duration of 500 fs (FWHM), waist size of 50 µm, energy of 12 J ($a_0 = 7$) wavelength 0.8 µm in (a) a uniform plasma (b) a plasma with transverse parabolic profile defined by $a = 1.5 \times 10^{29}$ m^{-5}.

For a plasma density of $1 \times 10^{17}\,\mathrm{cm}^{-3}$, a laser pulse with a waist size of 100 µm and energy of 100 J ($a_0 = 10$) produces a 210 MeV electron beam with 41% energy spread, 23 nC charge and 60 µm bunch length after 16 mm propagation (Fig. 7a). If only the high-energy peak is selected (240 MeV $< E <$ 340 MeV), the mean energy is 290 MeV, with 7% energy spread and 18 nC charge. If the laser energy is increased to 400 J ($a_0 = 20$), the high-energy peak (0.8 GeV $< E <$ 1.4 GeV) has a mean energy of 1.1 GeV, with 12% energy spread and 180 nC charge after 26 mm propagation (Fig. 7b). For $n_e = 2.5 \times 10^{16}\,\mathrm{cm}^{-3}$, $w_0 = 200\,\mu\mathrm{m}$ and $E_{laser} = 400\,\mathrm{J}$ ($a_0 = 10$), the high-energy peak (1.2 GeV $< E <$ 2 GeV) has a mean energy of 1.6 GeV with 11% energy spread and 130 nC charge after 80 mm propagation (Fig. 7c). The electron beam energy can be increased further using $n_e = 1 \times 10^{16}\,\mathrm{cm}^{-3}$, $w_0 = 300\,\mu\mathrm{m}$ and $E_{laser} = 430\,\mathrm{J}$ ($a_0 = 7$), which results in a high-energy peak (1 GeV $< E <$ 2.5 GeV) with a mean energy of 1.7 GeV, 19% energy spread and 145 nC charge after 205 mm propagation (Fig. 7d). In some cases the energy spread is narrower if acceleration is stopped before dephasing.

We also performed simulations for waist sizes smaller than 100 µm, as shown in Fig. 8. Under these conditions, which are closer to the waist sizes normally employed when using near-infrared lasers, the accelerator performance is better for high plasma densities. For a beam waist of 25 µm and a plasma density of $2 \times 10^{17}\,\mathrm{cm}^{-3}$, electrons are produced with energy up to about 260 MeV and charge up to about 330 nC in a 6–13 mm long plasma. If the beam waist is increased to 50 µm, the maximum energy is about 650 MeV with a charge of 350 nC in a 25 mm long plasma with density of $1 \times 10^{17}\,\mathrm{cm}^{-3}$. Further increasing the plasma density results in degradation of the accelerator performance because at the wavelength $\lambda_0 = 10.6\,\mu\mathrm{m}$ the critical plasma density is $9.9 \times 10^{18}\,\mathrm{cm}^{-3}$, in contrast with $1.7 \times 10^{21}\,\mathrm{cm}^{-3}$ at $\lambda_0 = 0.8\,\mu\mathrm{m}$. At lower plasma densities, on the other hand, the accelerator performance is limited by diffraction. For example, for $n_e = 2.5 \times 10^{16}\,\mathrm{cm}^{-3}$ a laser pulse with a waist size of 50 µm and an energy of 12 J ($a_0 = 7$) produces a 170 MeV electron beam with 60% energy spread and 0.5 nC charge in a length of 61 mm (Fig. 9a). When using external guiding, the energy increases to 290 MeV with 11 nC charge in a length of 72 mm (Fig. 9b).

Scaling laws

We have compared the results of our PIC simulations with the predictions of analytical formulas based on phenomenological [16] and similarity [17] theories. These simplified models use laser and plasma parameters that aim to enhance the accelerator performance and minimise the evolution of the laser pulse and accelerator cavity, which is assumed to be approximately spherical. In reference [16] the matched condition is

$$k_p R \approx k_p w_0 \approx 2\sqrt{a_0}, \tag{1}$$

with R the bubble radius. Reference [17] uses

$$k_p R \approx k_p w_0 \approx 1.12\sqrt{a_0}. \tag{2}$$

Here simulations have been performed for a wide range of parameters that are not necessarily matched. We find that a_0 and the bubble size evolve significantly as the laser propagates in the plasma, as shown for example in Fig. 2. Typically, the bubble expands longitudinally, occasionally more than doubling in size. The bubble transverse size often grows by more than 50%. After performing fits of the simulation results we found that the average bubble size is approximately

$$R \approx R_0 \sqrt{\frac{\lambda_0[\mu\mathrm{m}]}{10.6}}\, P[\mathrm{TW}]^{1/4} \left(\frac{10^{18}}{n_e[\mathrm{cm}^{-3}]}\right)^{1/3}, \tag{3}$$

with $R_0 \approx 17\,\mu$m for the transverse bubble size and $R_0 \approx 22\,\mu$m for the longitudinal size. The dependence on w_0 has been neglected because it is weak for $w_0 \gtrapprox 50\,\mu$m. For low plasma densities this formula slightly overestimates the bubble size. A sample fit is shown in Fig. 10.

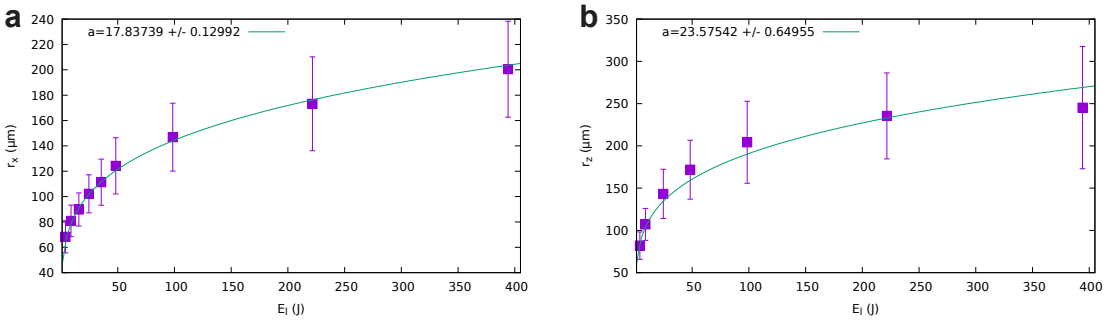

Figure 10: Bubble size versus laser energy for a plasma with density of $1 \times 10^{17}\,\mathrm{cm}^{-3}$ and a laser pulse with a wavelength of 10.6 μm, pulse duration of 500 fs (FWHM) and waist size of 100 μm. a) Bubble size in the laser polarisation plane. b) Longitudinal bubble size.

Energy scaling

Reference [16] predicts that the electron beam energy scales approximately as

$$E \approx \epsilon_{av} k_p L_{acc} m_e c^2, \tag{4}$$

where m_e is the electron mass, ϵ_{av} the average accelerating field and L_{acc} the acceleration length. When the acceleration is limited by dephasing, $\epsilon_{av} = \sqrt{a_0}/2$ and

$$L_{acc} \approx \frac{2}{3}\frac{\omega_0^2}{\omega_p^2} R. \tag{5}$$

This assumption is compatible with most of our results, except for simulations limited by diffraction, such as for low plasma densities and low laser energies. Eq. 4 can be rewritten using Eq. 3 (with $R_0 = 19.5\,\mu$m) and Eq. 5, obtaining

$$E[\mathrm{MeV}] \approx 52 \frac{10.6}{\lambda_0[\mu\mathrm{m}]} \frac{\sqrt{P[\mathrm{TW}]}}{\sqrt{w_0[\mu\mathrm{m}]}} \left(\frac{10^{18}}{n_e[\mathrm{cm}^{-3}]}\right)^{5/6}, \tag{6}$$

which reproduces our simulation results well. The predicted energies are typically higher than the mean values shown in Fig. 5 and Fig. 8, but these are weighted down by the low-energy tail and do not represent the energy of the quasi-monoenergetic peaks. Further details on the dependence on the laser waist size and pulse duration are provided in the following sections.

Charge scaling

Reference [16] estimates that under matched conditions (Eq. 1) the number of accelerated electrons is

$$N \approx 2.5 \times 10^9 \frac{\lambda_0[\mu\mathrm{m}]}{0.8} \sqrt{\frac{P[\mathrm{TW}]}{100}}. \tag{7}$$

Reference [17] predicts a similar scaling, but with a different proportionality factor and matched condition (Eq. 2). The derivation of Eq. 7 is based on the assumption that electrons absorb all the electromagnetic field energy contained in the accelerating cavity and an equal amount of plasma kinetic energy, which both scale as $(k_p R)^5$. Such a strong dependence on R implies that small changes in bubble size produce large variations in charge. In our simulations, the bubble is often longitudinally elongated and its size and shape evolve significantly during propagation in the plasma, as shown in Fig. 2. Eq. 7 underestimates the charge and does not reproduce the scaling with the laser and plasma parameters that have been observed. Most results presented here agree with the formula

$$N \approx 9 \times 10^{10} \frac{\lambda_0[\mu\mathrm{m}]}{10.6} E_{laser}^{\delta}[\mathrm{J}] \sqrt{\frac{n_e[\mathrm{cm}^{-3}]}{10^{18}}}, \tag{8}$$

where the parameter δ depends on the plasma density and laser waist size. Fits of the simulation results indicate that $\delta \approx 3/4$ for $n_e \gtrapprox 2.5 \times 10^{16}\,\mathrm{cm}^{-3}$ and $w_0 \gtrapprox 100\,\mu\mathrm{m}$. For $w_0 < 100\,\mu\mathrm{m}$, δ decreases, down to about $1/2$ for $w_0 = 25\,\mu\mathrm{m}$.

Bunch length scaling

The bunch length scales as

$$\sigma_z[\mu\mathrm{m}] \approx 33\, E_{laser}^{\delta_z}[\mathrm{J}], \tag{9}$$

where $\delta_z \approx \delta^{1/3}$. The transverse beam size follows a similar scaling with energy, but it also increases with the waist size and plasma density. The beam performs betatron oscillations and is typically larger along the laser polarisation plane. Interaction with the laser can introduce additional modulations, especially for long pulse durations. The charge density is also difficult to estimate, due to bunch sub-structure.

Validity range

In general, we found that the scaling laws presented here reproduce results obtained for densities $n_e \gtrapprox 2.5 \times 10^{16}\,\mathrm{cm}^{-3}$, $w_0 \gtrapprox 50\,\mu\mathrm{m}$ and laser pulse durations between 250 fs and 750 fs. They are not accurate close to the threshold for injection, and also when self-guiding is less effective, such as for $n_e = 1 \times 10^{16}\,\mathrm{cm}^{-3}$ and $T_{FWHM} = 125\,\mathrm{fs}$. A comprehensive study of the bunch

structure, transverse beam size and emittance would require simulations with a larger number of azimuthal modes and higher resolution than performed here.

Dependence on laser beam waist

Results presented in the previous sections show that a LWFA driven by a CO_2 laser can be operated using a wide range of laser waist sizes. When using near-infrared lasers, it is usually recommended to match the waist and bubble size (Eq 1, 2) [16, 17]. Here we directly investigated the dependence of the electron beam properties on w_0 for a CO_2 laser pulse with fixed power.

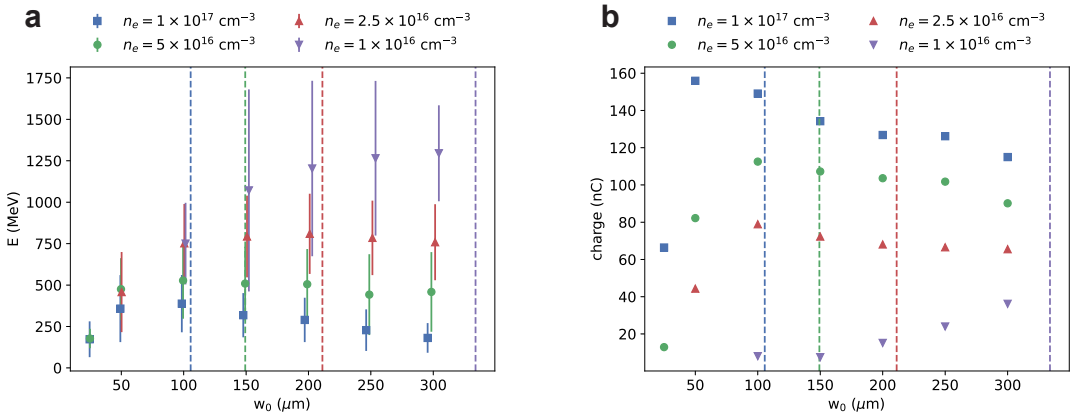

Figure 11: (a) Mean energy and (b) charge of electron beams produced in a pre-ionised plasma of varying density by a laser pulse with duration of 500 fs (FWHM), energy of 100 J, wavelength of 10.6 µm and varying waist size. Vertical lines mark the plasma wavelength λ_p. Error bars correspond to the r.m.s. energy spread.

Fig. 11 shows the mean energy (a) and charge (b) of electron beams generated in a uniform plasma with a density between $1 \times 10^{16}\,\mathrm{cm}^{-3}$ and $1 \times 10^{17}\,\mathrm{cm}^{-3}$ by a laser pulse with 500 fs duration, 100 J energy ($P = 200$ TW) as a function of beam waist size. The corresponding a_0 ranges from 3.3 to 40. For all densities, the highest electron energy is obtained when $w_0 \approx \lambda_p$, with λ_p the plasma wavelength, which is marked by the vertical lines in the plot. For the chosen laser power, the average bubble size is also close to λ_p (Eq. 3). The charge follows a different trend, as shown in Fig. 11b. It drops sharply for small w_0, when the accelerator performance is limited by diffraction, and it decreases slowly for large w_0 and $n_e \gtrapprox 2.5 \times 10^{16}\,\mathrm{cm}^{-3}$. The efficiency has a maximum of about 55% close to $w_0 = 100\,\mu$m for densities down to $2.5 \times 10^{16}\,\mathrm{cm}^{-3}$, and is about 10% for $1 \times 10^{16}\,\mathrm{cm}^{-3}$ and the selected w_0 range. For $n_e \gtrapprox 5 \times 10^{16}\,\mathrm{cm}^{-3}$ the spot size, divergence and emittance are slightly smaller when $w_0 \approx \lambda_p$, but for lower densities the dependence on w_0 is weaker and sometimes better results are obtained when $w_0 < \lambda_p$. Simulations performed for higher laser energy, when the bubble size $R > \lambda_p$, predict that the maximum electron energy is still obtained when $w_0 \approx \lambda_p$, but the drop in charge for small beam waists is reduced.

Dependence on laser pulse duration

Self-guiding in a plasma is expected to be more efficient when $T_{FWHM} \approx \lambda_p/c$. For shorter pulse durations, the refractive index modification leading to self-focusing may occur too slowly to guide the front of the laser pulse. For longer pulse durations, instabilities can develop [18]. Here we study the dependence of the electron beam properties on the pulse duration for a fixed beam waist, adjusting the laser energy to keep the power constant.

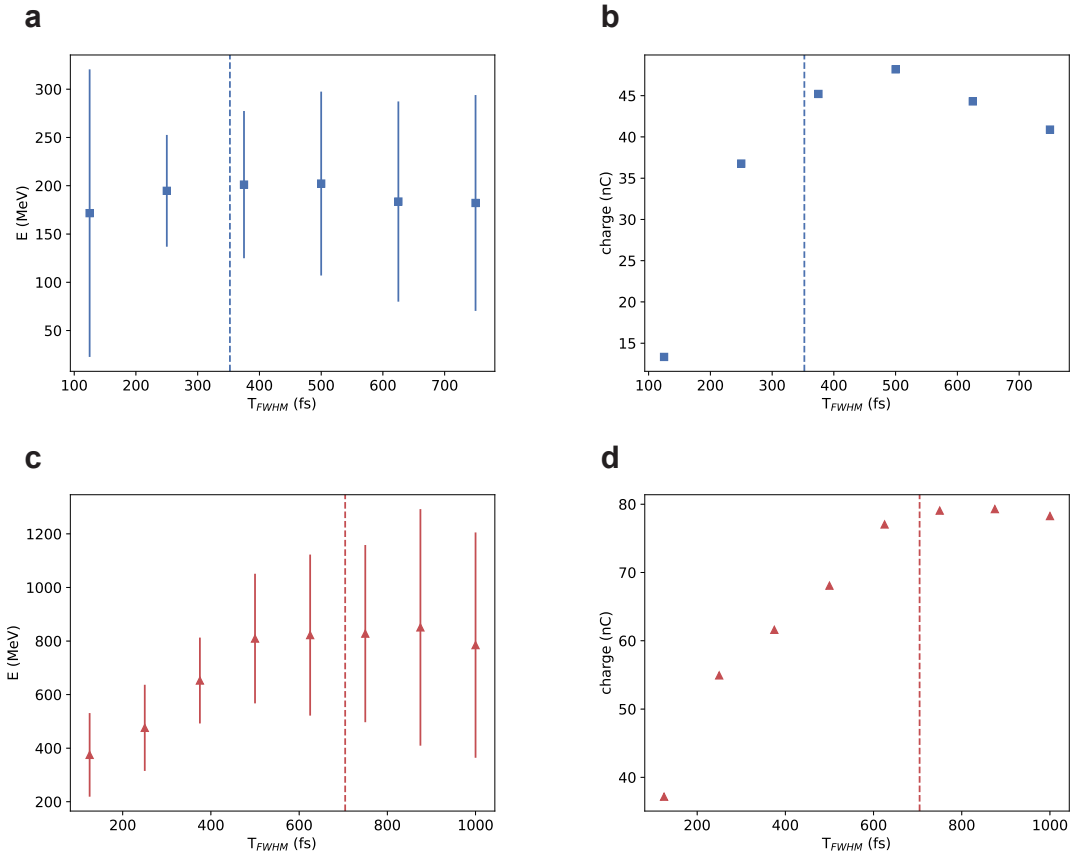

Figure 12: (a,c) Mean energy and (b,d) charge of electron beams produced in a pre-ionised plasma by a laser pulse with wavelength of 10.6 µm, $a_0 = 5$ and varying duration. The plasma density and laser waist size are: (a-b) 1×10^{17} cm^{-3} and 100 µm; (c-d) 2.5×10^{16} cm^{-3} and 200 µm. Vertical lines mark the plasma wavelength λ_p. Error bars correspond to the r.m.s. energy spread.

Fig. 12 shows the mean energy and charge of electron beams generated by a laser pulse with varying duration and $a_0 = 5$. In Fig. 12a-b the waist size is 100 µm, which is matched to the plasma density of 1×10^{17} cm^{-3}, as shown in the previous section. The corresponding laser power is 50 TW, with energy between 6 J and 24 J. The laser beam remains focused past the dephasing length for all pulse durations considered, resulting in approximately the same final electron energy, as shown in Fig. 12a. The mean energy is slightly higher and the energy spread narrower when $T_{FWHM} \approx \lambda_p/c$, which is marked by the vertical line in the plot. The charge increases with pulse duration, because of the higher laser energy, but slowly decreases for $T_{FWHM} > \lambda_p/c$. The bunch length, transverse beam size, emittance and divergence also

increase with pulse duration. The efficiency is peaked at 250 fs and ranges from 35% to 50%. For long pulse durations the front of the electron bunch can interact with the back of the laser pulse, which causes beam degradation, but can boost the emission of betatron radiation [19].

Fig. 12c-d shows the mean energy and charge generated in a plasma with density of $2.5 \times 10^{16}\,\mathrm{cm}^{-3}$ by a laser pulse with matched spot size $w_0 = 200\,\mu\mathrm{m}$ and $a_0 = 5$, which corresponds to a power $P = 190\,\mathrm{TW}$ and energy between 25 J and 200 J. For short pulse durations, the accelerator performance is limited by diffraction and the electron energy increases linearly with T_{FWHM}, until dephasing is reached at about 500 fs. The charge forms a plateau at $T_{FWHM} \approx \lambda_p/c$. The efficiency is peaked at 500 fs and ranges from 44% to 54%.

Discussion

We have performed PIC simulations of a LWFA driven by a 10.6 µm laser generating sub-picosecond pulses with powers of 10s–100s TW. Results indicate that electron beams with 100s MeV to GeV energy and 1–100s nC charge can be produced in a pre-ionised uniform plasma with density of 10^{16}–$10^{17}\mathrm{cm}^{-3}$, using no external guiding, with a laser to electron beam efficiency that can exceed 50%. For example, a 20 TW CO_2 laser emitting pulses with 500 fs duration and 10 J energy focused to a waist size of 50 µm into a plasma with density of $1 \times 10^{17}\,\mathrm{cm}^{-3}$ and length of 16 mm produces an electron beam with mean energy of 230 MeV with 4% energy spread, 4 nC charge and 14 mrad r.m.s. divergence, selecting only the high-energy peak. If the laser energy is increased to 100 J ($P = 200\,\mathrm{TW}$), the spot size to $w_0 = 100\,\mu\mathrm{m}$, and the plasma length is set to 20 mm, the mean energy of the selection is 560 MeV with 7% energy spread, 50 nC charge and 15 mrad r.m.s. divergence. If the laser energy is further increased to 400 J ($P = 800\,\mathrm{TW}$), with $w_0 = 200\,\mu\mathrm{m}$, $n_e = 2.5 \times 10^{16}\,\mathrm{cm}^{-3}$ and a plasma length of 86 mm, the mean energy of the selection is 1.6 GeV with 12% energy spread, 140 nC charge and 6 mrad r.m.s. divergence. Such charge levels are significantly higher than what is expected from near-infrared lasers of similar power, although the bunch length and emittance can be larger. Nevertheless, currents of 100s kA are achievable. These results have been obtained in a pre-ionised plasma, but simulations performed using neutral helium indicate that a CO_2 laser can fully ionise the gas. Alternative schemes, such as plasma discharge waveguides [15] or heater pulses [20] can also be considered, especially for low laser powers. Here no attempt has been made to optimise parameters such as emittance, energy spread and bunch duration, but techniques such as down-ramp injection [21] and density modulation [22] could be used to control injection and the properties of the beam. Moreover, techniques based on ionisation injection [23] could further boost the beam charge and efficiency.

We have shown that a wide range of laser waist sizes and pulse durations can be employed, but the electron beam energy is maximised when $w_0 \approx \lambda_p$ and $T_{FWHM} \approx \lambda_p/c$. The charge, on the other hand, is typically maximised for slightly smaller waist sizes and longer pulse durations. However, self-guiding is often less effective for waist sizes smaller than 50 µm and pulse durations shorter than 250 fs, resulting in lower electron beam energies and charges, especially for low plasma densities and low laser energies. Under these conditions, external guiding can significantly enhance the electron beam energy. On the other hand, pulse durations

approaching 1 ps can degrade the electron beam quality due to interaction with the laser field, but could potentially boost the emission of betatron radiation.

With advances in CO_2 laser technology, as discussed in the next Chapter, LWFAs driven by CO_2 lasers could be ideal for applications that require high-charge electron beams, such as industrial imaging, activation analysis, radioisotope production and radiotherapy. A bright tunable X-ray source could also be realised using Compton back-scattering [24]. An optically pumped CO_2 laser driven LWFA would be efficient, compact, robust and could be made mobile.

Bibliography

[1] T. Tajima and J. M. Dawson, "Laser Electron Accelerator," *Physical Review Letters*, vol. 43, pp. 267–270, July 1979.

[2] E. Esarey, C. B. Schroeder, and W. P. Leemans, "Physics of laser-driven plasma-based electron accelerators," *Reviews of Modern Physics*, vol. 81, pp. 1229–1285, Aug. 2009.

[3] D. Bauer, P. Mulser, and W. H. Steeb, "Relativistic Ponderomotive Force, Uphill Acceleration, and Transition to Chaos," *Phys. Rev. Lett.*, vol. 75, pp. 4622–4625, Dec. 1995.

[4] I. Pogorelsky, "Prospects for laser wakefield accelerators and colliders using CO2 laser drivers," *Nuclear Instruments and Methods in Physics Research Section A: Accelerators, Spectrometers, Detectors and Associated Equipment*, vol. 410, pp. 524–531, June 1998.

[5] R. N. Campbell, E. Brunetti, S. R. Yoffe, and D. A. Jaroszynski, "Optical pumped ultrashort pulse CO2 lasers as drivers of laser-plasma accelerators and other applications," in *XXII International Symposium on High Power Laser Systems and Applications* (P. Di Lazzaro, ed.), (Frascati, Italy), p. 46, SPIE, Jan. 2019.

[6] M. C. Downer, R. Zgadzaj, A. Debus, U. Schramm, and M. C. Kaluza, "Diagnostics for plasma-based electron accelerators," *Rev. Mod. Phys.*, vol. 90, p. 035002, Aug. 2018.

[7] M. R. Islam, E. Brunetti, R. P. Shanks, B. Ersfeld, R. C. Issac, S. Cipiccia, M. P. Anania, G. H. Welsh, S. M. Wiggins, A. Noble, R. A. Cairns, G. Raj, and D A Jaroszynski, "Near-threshold electron injection in the laser–plasma wakefield accelerator leading to femtosecond bunches," *New Journal of Physics*, vol. 17, p. 093033, Sept. 2015.

[8] E. Brunetti, R. P. Shanks, G. G. Manahan, M. R. Islam, B. Ersfeld, M. P. Anania, S. Cipiccia, R. C. Issac, G. Raj, G. Vieux, G. H. Welsh, S. M. Wiggins, and D. A. Jaroszynski, "Low Emittance, High Brilliance Relativistic Electron Beams from a Laser-Plasma Accelerator," *Phys. Rev. Lett.*, vol. 105, p. 215007, Nov. 2010.

[9] S. P. D. Mangles, C. D. Murphy, Z. Najmudin, A. G. R. Thomas, J. L. Collier, A. E. Dangor, E. J. Divall, P. S. Foster, J. G. Gallacher, C. J. Hooker, D. A. Jaroszynski, A. J. Langley, W. B. Mori, P. A. Norreys, F. S. Tsung, R. Viskup, B. R. Walton, and K. Krushelnick, "Monoenergetic beams of relativistic electrons from intense laser–plasma interactions," *Nature*, vol. 431, pp. 535–538, Sept. 2004.

[10] C. G. R. Geddes, C. Toth, J. van Tilborg, E. Esarey, C. B. Schroeder, D. Bruhwiler, C. Nieter, J. Cary, and W. P. Leemans, "High-quality electron beams from a laser wakefield accelerator using plasma-channel guiding," *Nature*, vol. 431, pp. 538–541, Sept. 2004.

[11] J. Faure, Y. Glinec, A. Pukhov, S. Kiselev, S. Gordienko, E. Lefebvre, J.-P. Rousseau, F. Burgy, and V. Malka, "A laser–plasma accelerator producing monoenergetic electron beams," *Nature*, vol. 431, pp. 541–544, Sept. 2004.

[12] W. P. Leemans, B. Nagler, A. J. Gonsalves, C. Tóth, K. Nakamura, C. G. R. Geddes, E. Esarey, C. B. Schroeder, and S. M. Hooker, "GeV electron beams from a centimetre-scale accelerator," *Nature Physics*, vol. 2, pp. 696–699, Oct. 2006.

[13] A. J. Gonsalves, K. Nakamura, J. Daniels, C. Benedetti, C. Pieronek, T. C. H. de Raadt, S. Steinke, J. H. Bin, S. S. Bulanov, J. van Tilborg, C. G. R. Geddes, C. B. Schroeder, C. Tóth, E. Esarey, K. Swanson, L. Fan-Chiang, G. Bagdasarov, N. Bobrova, V. Gasilov, G. Korn, P. Sasorov, and W. P. Leemans, "Petawatt Laser Guiding and Electron Beam Acceleration to 8 GeV in a Laser-Heated Capillary Discharge Waveguide," *Phys. Rev. Lett.*, vol. 122, p. 084801, Feb. 2019.

[14] R. Lehe, M. Kirchen, I. A. Andriyash, B. B. Godfrey, and J.-L. Vay, "A spectral, quasi-cylindrical and dispersion-free Particle-In-Cell algorithm," *Computer Physics Communications*, vol. 203, pp. 66–82, June 2016.

[15] D. J. Spence and S. M. Hooker, "Investigation of a hydrogen plasma waveguide," *Phys. Rev. E*, vol. 63, p. 015401, Dec. 2000.

[16] W. Lu, M. Tzoufras, C. Joshi, F. S. Tsung, W. B. Mori, J. Vieira, R. A. Fonseca, and L. O. Silva, "Generating multi-GeV electron bunches using single stage laser wakefield acceleration in a 3D nonlinear regime," *Physical Review Special Topics - Accelerators and Beams*, vol. 10, June 2007.

[17] S. Gordienko and A. Pukhov, "Scalings for ultrarelativistic laser plasmas and quasimonoenergetic electrons," *Physics of Plasmas*, vol. 12, p. 043109, Apr. 2005.

[18] E. Esarey, P. Sprangle, J. Krall, and A. Ting, "Self-focusing and guiding of short laser pulses in ionizing gases and plasmas," *IEEE J. Quantum Electron.*, vol. 33, no. 11, pp. 1879–1914, Nov./1997.

[19] S. Cipiccia, M. R. Islam, B. Ersfeld, R. P. Shanks, E. Brunetti, G. Vieux, X. Yang, R. C. Issac, S. M. Wiggins, G. H. Welsh, M.-P. Anania, D. Maneuski, R. Montgomery, G. Smith, M. Hoek, D. J. Hamilton, N. R. C. Lemos, D. Symes, P. P. Rajeev, V. O. Shea, J. M. Dias, and D. A. Jaroszynski, "Gamma-rays from harmonically resonant betatron oscillations in a plasma wake," *Nature Phys*, vol. 7, pp. 867–871, Nov. 2011.

[20] N. A. Bobrova, P. V. Sasorov, C. Benedetti, S. S. Bulanov, C. G. R. Geddes, C. B. Schroeder, E. Esarey, and W. P. Leemans, "Laser-heater assisted plasma channel formation in capillary discharge waveguides," *Physics of Plasmas*, vol. 20, p. 020703, Feb. 2013.

[21] M. Hansson, B. Aurand, X. Davoine, H. Ekerfelt, K. Svensson, A. Persson, C.-G. Wahlström, and O. Lundh, "Down-ramp injection and independently controlled acceleration of electrons in a tailored laser wakefield accelerator," *Phys. Rev. ST Accel. Beams*, vol. 18, p. 071303, July 2015.

[22] M. P. Tooley, B. Ersfeld, S. R. Yoffe, A. Noble, E. Brunetti, Z. M. Sheng, M. R. Islam, and D. A. Jaroszynski, "Towards Attosecond High-Energy Electron Bunches: Controlling Self-Injection in Laser-Wakefield Accelerators Through Plasma-Density Modulation," *Phys. Rev. Lett.*, vol. 119, p. 044801, July 2017.

[23] C. McGuffey, A. G. R. Thomas, W. Schumaker, T. Matsuoka, V. Chvykov, F. J. Dollar, G. Kalintchenko, V. Yanovsky, A. Maksimchuk, K. Krushelnick, V. Y. Bychenkov, I. V. Glazyrin, and A. V. Karpeev, "Ionization Induced Trapping in a Laser Wakefield Accelerator," *Physical Review Letters*, vol. 104, Jan. 2010.

[24] K. Ta Phuoc, S. Corde, C. Thaury, V. Malka, A. Tafzi, J. P. Goddet, R. C. Shah, S. Sebban, and A. Rousse, "All-optical Compton gamma-ray source," *Nature Photon*, vol. 6, pp. 308–311, May 2012.

[25] M.-C. Vozenin, J. Hendry, and C. Limoli, "Biological Benefits of Ultra-high Dose Rate FLASH Radiotherapy: Sleeping Beauty Awoken," *Clinical Oncology*, vol. 31, pp. 407–415, July 2019.

Conceptual design, and costing outline, of a 10 μm, 5-10 TW ultra-short-pulse, high repetition-rate and high energy scalable laser

The approach considered is a hybrid, or tandem pumped, diode pumped solid-state (DPSS) pumped CO_2 laser system. Optically pumping at raised CO_2 pressures enables continuous tunability because of pressure-induced overlapping of neighbouring ro-vibrational transitions. This overlaying, within the spectral domain, of the ro-vibrational transition structures, is further augmented by the ability to exploit arbitrary gas mixes of CO_2 molecular isotopologues (in species and proportion). This is possible in principle provided certain criteria are met. These together provide a path to continuous tunability, or engineering of broadband gain structures, that were hitherto unattainable in CO_2 lasers operating at comparable pressures. This capability presents a route to, at least, sub-saturation amplification of an ultra-short pulse (USP) without significant gain induced spectral narrowing, given an appropriately engineered gain distribution. For the saturation to above saturation amplification regime, amplification of pulses of pulse durations longer than the cross relaxation time constant within the inhomogenously, ro-vibrationally broadened gain distribution of CO_2, require care, but options exist. The implications for an USP system at ≈ 10 μm are clear because of the inequality $\Delta\nu\Delta t \geq K$ ($\Delta\nu$ = FWHM), provided multi-isotopologue molecular gas mixes are used. Employing a DPSS system front-end, as pump, and for pumped medium conditions such that excessive ν_3 mode vibrational temperatures (T_3) are not induced or required in the generation of reasonable gain at useful volumetric extraction, utilization of materials of acceptably high activation energy for the suppression of dissociative adsorption of CO_2 [1], the explicit absence of discharge excitation and thus molecular dissociation and a necessary catalyser, and sputter driven gas contamination related deposition on optical components, opens the path to near indefinite shelf and dynamic multi-isotopologue gas lifetime systems. Viable gas kinetic, or vibrational T_3, temperature limits are governed by a Maxwellian gas at room temperature, but at elevated ν_3 mode vibrational temperatures, then for an assumed Steric factor, and estimates of unacceptable molecular dissociation onset is established an acceptable upper T_3 magnitude (similar to results reported in reference [2]). In addition, evolution of the Treanor distribution associated sequence band populations with T_3 provides further confirmation of the presence of an acceptable upper bound vibrational temperature if preservation of this capability of arbitrary multi-isotopologue mix utilization is desired. It is estimated that the absolute permitted T_3 upper bound is to be found at ≈ 2000 K, with perhaps a practical limit at ≈ 1800 K. Given T_3 as a system design constraint, then any reduction in CO_2 partial pressures will directly result in corresponding reductions in small

signal gain, and volumetric extraction. The ability to practically exploit high CO_2 partial pressures in a DPSS-CO_2 OPML device is very favourable. It is therefore possible to create a uniquely capable and truly sealed and robust device. Utilization of arbitrary rare isotope molecular isotopologue CO_2 mixes, in species and proportion, would otherwise be neither affordable nor sustainable because of dissociation-recombination statistical mixing processes. The specific employment of a DPSS system front end, which is matched to CO_2 pump transitions corresponding to useful pump absorption scale lengths at high CO_2 partial pressures, without dilution or detuning, is favourable because of near resonant collisional CO_2 energy exchange, for both pump and emission bands and, where the more satisfactory CO_2-CO_2 collisional broadening coefficient to that of CO_2-He or CO_2-N_2 for example is also relevant [3,4]. The recently Arshinov et al., [4] reported on the relevant CO_2-CO_2 coefficient and the possible benefit of the 30% enhancement over the long standing generally utilized 'standard' CO_2 pressure broadening coefficient is notable. This would further advantage implementation of arbitrary molecular isotopologue mixes. From a system design perspective, the pressure broadening coefficients of possible buffer gases are reported. The temperature dependence is irrelevant to pulsed laser operation in general. Pulsed discharges are temporally typically near constant volume and significant heating is undesirable.

The device being considered here is an OPML (Optically Pumped Molecular Laser), with a front-end driver comprising a suitable DPSS laser source. The suitability of a DPSS source in this context is defined by: any energy based system cannot perform better than the energy related efficiency of its most efficient constitutive element or primary energy source. The DPSS front-end sets the system-wide performance ceiling *i.e.* a DPSS-OPML depends on its DPSS front-end. The availability of suitable DPSS pump sources, for a given OPML gas selection that gives a spectrally useful output enables the DPSS-OPML system. For this approach to be viable, affordable and practical, a number of criteria must be met.

(i) The DPSS source dopant medium within typical substrates must have an extended excited level lifetime that permits laser diode (LD) pumping affordably. That is from an affordable laser diode array.

(ii) Ideally, the dopant medium should have a modest emission cross section, which enables good energy storage.

(iii) The diode laser pumped medium's quantum defect must be as small as possible.

(iv) Spectrally, the LD pump DPSS source gain spectral distribution must include the pump band(s) of the OPML gas medium mix under consideration. This is eased in this case by pressure broadening of the ro-vibrational transitions of the OPML gas medium, which coalesces then into contiguous pump bands. This is open to augmentation using an arbitrary molecular isotopologue mix, assisted by the rapid inter molecular V↔V energy exchange of relevant vibrational quanta, regardless of whether the mix is only pumped on a transition of one of the mix component isotopologues. [5]

(v) The DPSS dopant medium within substrate(s) own pump bands must match the spectral output character of commercial and affordable high power laser diode bars.

(vi) The dopant medium in substrate(s) must be commercially available in a suitable form factor *e.g.* bulk, fibre, thin disc and thin slab, to the scale required.

(vii) The dopant should be compatible with substrates of reasonable room temperature (RT) thermal conductivity and thermo-optic coefficient. The substrates should ideally display respectively enhancement and reduction in these parameters with decreasing temperature, thereby not excluding cryogenic use, and perhaps benefitting from it.

The OPML gas medium of choice for this DPSS-OPML option is CO_2 because of its spectrum, wide commercial utility, significant research value, and the range of stable molecular isotopologues available, that is compared to the known performance, capability and platform limitations of current CO_2 laser technology (which is at the end of its meaningful development cycle).

DPSS-CO_2 is a suitable USP laser technology that will enable extreme light research and many other applications. The DPSS plus CO_2 OPML of this proposal admits two distinct pump path options. The **first** is direct pumping of the CO_2 transition(s), or a combination of transitions of a multi-isotopologue gas mix. The **second** is an indirect pump path incorporating a resonant transfer from a donor to an acceptor (*i.e.* CO_2).

The concept design described here addresses the first, direct pump case, which has already been demonstrated experimentally. Demonstration of the second pump path option is pending. The benefit of the second over the first is that the optical conversion efficiency can potentially be doubled. The optical to optical conversion efficiency of direct pumping limits at $\approx 20\%$, while indirect pumping is $\approx 40\%$. The latter represents the maximum feasible for CO_2 for lasing in the 10 μm spectral region. Historically, for this DPSS front end selection, indirect pumping has been the most obvious and lowest risk option. Nevertheless, direct pumping has been demonstrated and characterized, and is perhaps technically less challenging.

The media being considered for the DPSS front-end are the family of Tm:host doped media, which are not the sole options, but have significant merit. The DPSS-OPML driver has a spectrum suitable for both direct and indirect pump path options.

We now consider the CO_2 system output power amplifier stage and its characteristics. This will include determining the characteristics of the CO_2 preamp(s) and Tm:host CO_2 OPML driver requirement.

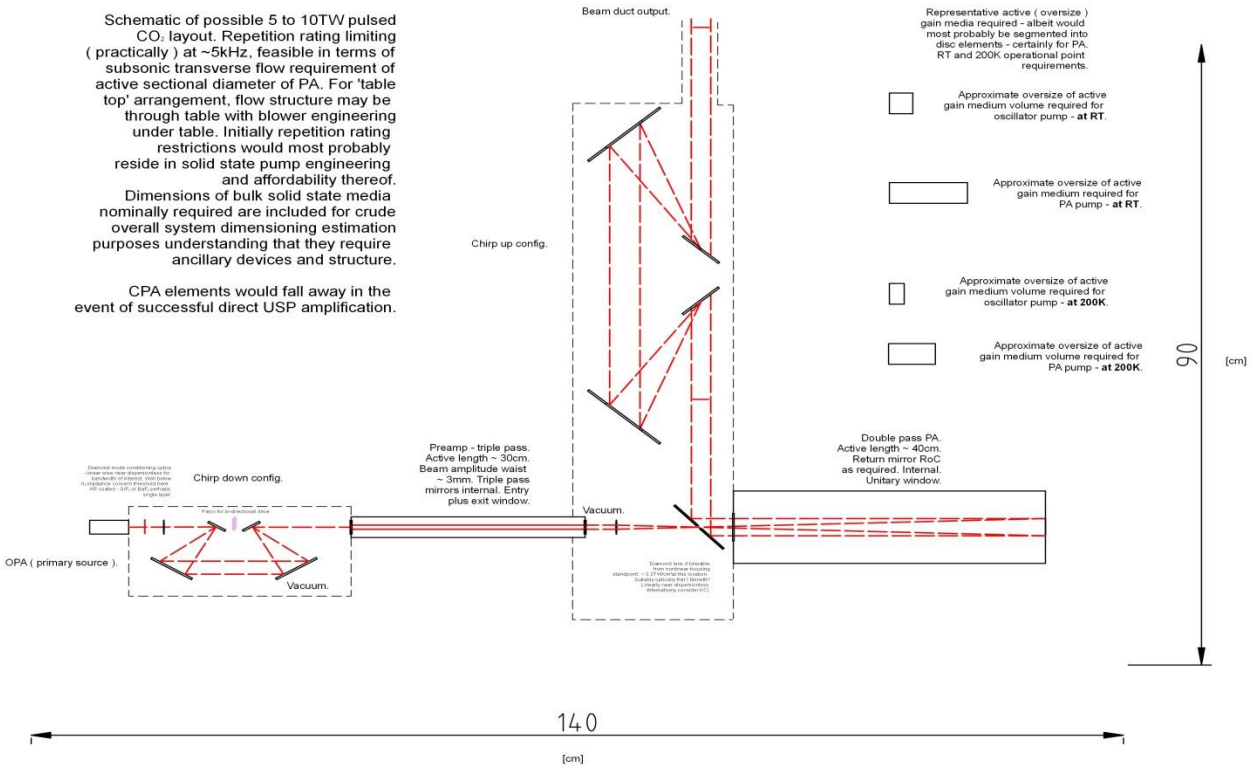

Figure 1: Schematic layout (roughly scaled). This shows only the CO_2 components of a system suitable for USP amplification. Aperture is scaled in preference to length. The approximate dimensions of the Tm:YAG active medium required are included. YAG is selected as a host medium for this study. However, it is not the only option, YAP, Y_2O_3, LuY_2O_3 [6,7] are also suitable, but are currently in various stages of availability and development.

The basis of the conceptual design is chirped pulse amplification (CPA), which is essential for high power USP amplification. A result of using CPA is that the systems are potentially more efficient, and moreover, self-focusing and other nonlinear processes are significantly reduced. We also consider the impact on the system geometry necessary to ensure suppression and management of undesired nonlinear processes. A roughly scaled schematic of the proposed general system layout is shown in Figure 1 and Figure 3. It is informative to compare this with the CO_2 component dimensions of just the BNL LWIR ATF Power Amplifier (Figure 3), which shows that it is a very large instrument comparatively.

Figure 2 Photograph of the BNL CO_2 power amplifier [8] .

To consider USP amplification, it is necessary to obtain a rough indication of the delay (τ_d) between coherent and incoherent responses. This can be approximately determined from the mean time between collisions of a molecule within the gas. At 5 atms, pure CO_2, at RT, $\tau_d \approx 44$ ps. This time constant is close to the ΔJ = +/-2 , +/-4 transition, in the case of a symmetric isotopologue, rotational relaxation time constant at the same pressure.

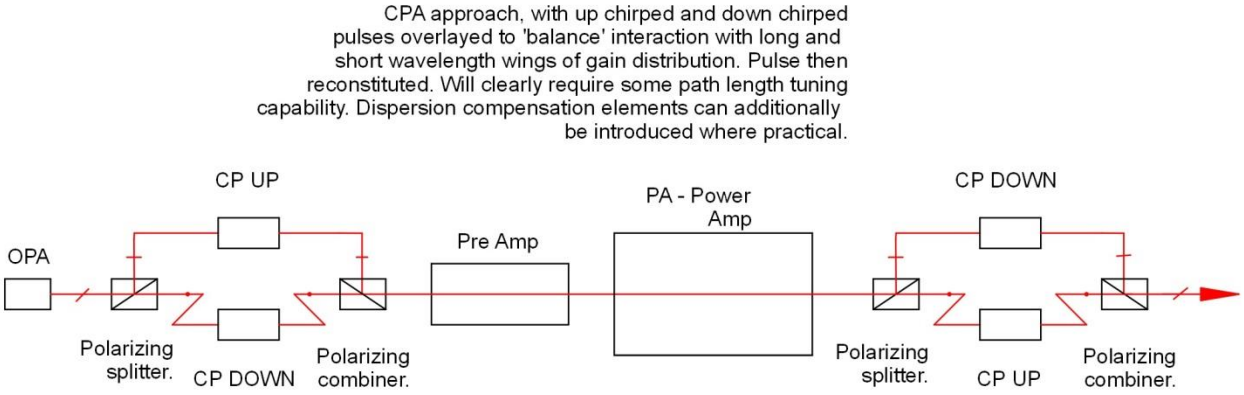

Figure 3: Schematic layout of alternative CPA laser system. In general for a top-hat pump profile and below saturation in the pre-amplifier, both pulse spectral and radial spatial distributions must be preserved. In latter case, chirping could in principle be implemented after the pre-amplifier, but would require finesse to implement effectively and a revised pump introduction relative to the Fig. 1 schematic, with the final output possibly randomly polarized, or perhaps with detail attention linear polarization recoverable. Polarization within amplifiers will be random.

In the case of direct amplification (non CPA) of an USP, then the rotational distribution is 'frozen' for the event, which results in the gain distribution being spectrally frozen. In the case of CPA, depending on the duration of the CPA pulse and assuming saturation or above saturation

(CO_2 saturation energy at the pressure concerned), the entire interacting pulse is temporally correlated with the chirped pulse, and the leading edge of the pulse during amplification may distort the spectral gain distribution profile dynamically during the interaction event, which distorts the trailing edge. This is equivalent to cross relaxation within the spectrally defined gain distribution of a solid state medium interacting with a chirped pulse. Therefore, pulse chirp rate needs to be limited for amplifiers approaching saturation, such as for the straightforward layout as depicted above in Figure 1. If a higher chirp rate is desired, a possible configurational solution does exist, as presented in the block diagram immediately below the comparative BNL PA depiction above in Figure 3. This aided by the spatial extent of the LWIR wavelength of interest here, as the nonlinear attributable pulse peak to leading or trailing edge spatial shift introduced on introductory layout power amplifier's transit would be, for a 100 ps chirped 2 J/cm^2 pulse, ≈ ($5\times10^{-3} + 2\times10^{-2}$ = diamond window double pass + gain length of ≈ 0.8 m contributions) of the median lasing wavelength. This corresponds to ≈ 2.5% of a wavelength. This estimate is based on the relevant values presented in the section below where non CPA nonlinear behaviour (≈ $n_2\times I\times L/\lambda$) is discussed. In terms of linear refractive index, diamond is essentially dispersion-less at 10 μm for a ≈ 1 ps spectral width event, where the attributable $\Delta n_{linear} \approx 4\times10^{-5}$, or ≈ 1×10^{-2} of the wavelength concerned for the in medium path length, or ≈ 1%, and for CO_2 at 5 atms, $\Delta n_{linear} \approx 3.7\times10^{-7}$, or ≈ 3×10^{-2} of the wavelength concerned for the in medium path length, or ≈ 3% (≈ $(\Delta n/\Delta\lambda)\times L\times(\Delta\lambda_{bandwidth}/\lambda)$) [9,10]. The induced shift is then ≈ 6% of the wavelength at 10μm. The interaction of the pulse with the gain medium would be spectrally balanced so that interaction with the inhomogeneously broadened gain distribution commences near simultaneously on both wings of the spectral distribution and converges on the pulse centre frequency, then progresses back to the wings. The question arises: what is the possible benefit of CPA, other than for laser induced damage threshold (LIDT) reduction and thus tolerance of optics and suppression of non-linear effects?

To return to the kinetics, the (100)↔(020) terminal levels relaxation interaction have a time constant of ≈ 1.4 ns-atm for CO_2 [11]. At 5 atms of pure CO_2, the relevant time constant is ≈ 280 ps. As a result, the lasing medium is no longer strictly two level, as population choking on a selected terminal level is mitigated by relaxation to the adjoining Fermi resonant level. Stretching the pulse to ≈ 1 ns would enhance this benefit further by introducing relaxation from the terminal pair (100)+(020) to the (010) level. The time constant for this process is generally understood to be of the order of 10 ns-atm for CO_2-CO_2 collisional interactions. Comparing with the preceding discussion, it should be noted that the PA of the BNL ATF LWIR system, the Optoel Piter 1 operates with a 1:0.5:8.5 CO_2:N_2:He 10 atm gas mix, giving ≈ 30 J in 10 ps, at a repetition rate of 0.1 Hz, with an efficiency of ≈ 0.6%. For this gas mix τ_d ≈ 15 ps [12]. More recent work suggests the 10 Bar (it is unclear if this is gauge or absolute) gas mix may have been modified to a 1:1.15:26.4 CO_2:N_2:He gas mix [13]. This is likely to have diminished the small signal gain, available volumetric extraction and efficiency. Despite this τ_d, BNL, according to its webpage [8] successfully amplifies a ≈ 50 ps stretched pulse, prior to compression. Their PA has 6 internal passes through the gain medium. The electrode length is ≈ 1 m, giving an internal structure longer than 1.5 m per pass through the gas fill, or ≈ 9 m. Further information on their site gives ≈ 70 ps as the

stretched pulse injected into their PA, with more than 6 passes internal to their PA gain medium. The hard aperture defined by the inter-electrode distance is ≈ 8 cm, which allows transmission of a Gaussian beam with ≈ 5 cm diameter (amplitude waist). Assuming a Gaussian, the peak irradiance for a 10 J, 25 ps pulse has an intensity of ≈ 0.04 TW/cm^2. This has been successfully implemented without apparently observing significant non-linear related self-focusing. This supports the scaling and viability of the system proposed in this report, in particular the following discussion in regards the obvious system constraints on direct USP amplification using a DPSS-CO_2 OPML. Finally, it should be remarked that the BNL final 10 atm PA, that has a window aperture diameter of at least 8 cm, compared with ≈ 5 atms and ≈ 2.5 cm, proposed here. For a systemically common engineering factor of safety of the window, a window material thickness at least 5 fold that of the system proposed here is required. This is significant as the non-linear pulse distortion within the associated solid state optics is larger than within the gaseous gain medium.

To evaluate the non CPA approach, the stretcher and compressor assemblies would be removed.

Non-CPA 10 μm amplifier at 1-2 TW/cm^2, with a gaseous gain medium and pressure containment windows.

10 μm driven stimulated Raman in diamond

Stimulated Raman amplification is unlikely, as Raman active level energy at ≈ 1332.8 cm^{-1} and 10 μm is ≈ 1000 cm^{-1}.

CO_2 and diamond molecular integrity at ≈ TW/cm^2 USP class irradiances for 10 μm

Molecular dissociation at these photon energies would require multiphoton interactions. An alternative, simplistic figure of merit is to consider dissociative 'evaporation' of the molecular structure in sufficiently strong fields. In both cases a threshold irradiance within the ≈ 10^{14} W/cm^2 range is indicated. This is two orders of magnitude in excess of what is under consideration.

2 μm pump driven Raman gain in diamond

Raman gain is g_r ≈ 2 cm/GW at ≈ 2 μm. Thus for the physical thicknesses of the diamond incorporated in the conceptual device, this is likely irrelevant, particularly given a broadband pump.

Nonlinear induced self-focusing contribution in diamond as a pressure containment window

As a first order estimate we consider that n_2 is likely <= 1×10^{-15} cm^2/W at 10 μm. Thus, as a worst case estimate at ≈ 1 TW/cm^2, the induced $\Delta n_2 \approx 1\times10^{-3}$. Or, considering a worst case of ≈ 2 TW/cm^2, $\Delta n_2 \approx 2\times10^{-3}$. Irradiance utilized is representative of the peak of the Gaussian distribution.

The thin window approximation gives a phase distortion that assumes linear polarization. For random polarization the distortion is less clear [14]:

$$f \approx \frac{n_0 (w_0)^2}{2L\Delta n_2},$$

where L is the length traversed, w_0 the amplitude waist, n_0 the linear refractive index, reducing to 1 in the thin window approximation for transitioning to an exterior with $n_0 \approx 1$.

(i) Thus for 1.3 mm thick diamond window of a PA (Modest assumption of rupture modulus and engineering factor of safety of 4. This could be made thinner), and $n_0 \approx 2.38$, an intra window $f \approx 9\times10^5 w_0^2$ for 1 TW/cm^2. And for 2 TW/cm^2 then $f \approx 4.6\times10^5 w_0^2$. Possibly worst case would be on 1st pass input through this window with an amplitude waist ≈ 2 mm (as that is the major scaling factor), 50 mJ nominally, so ≈ 0.8 TW/cm^2. Therefore, the intra window $f \approx 3.6$ m for ≈ 1 TW/cm^2, or for ≈ 0.8 TW/cm^2, 4.5 m. Extra window ≈ 1.5 m to 1.9 m. This does not highlight any concerns. On 2nd pass exit, for the USP 5.5 J case, with a 1.25 cm amplitude waist. This would peak at 2 TW/cm^2. $f \approx 72$ m for intra window because of the aperture scaling, and extra window $f \approx 30$ m. This is not of any concern. (Note: a diamond pressure containment window is transited only on entrance and exit as rear amp mirror is internal. The influence of amplitude waist scaling is significant.)

(ii) For a preamp, this is not an issue as only one window (the exit) is exposed to significant power density. The pre-amplifier exit window is also thinner and has a smaller aperture. In this case $w_0 \approx 3$ mm and output irradiance ≈ 0.35 TW/cm^2. A ≈ 0.7 mm thick diamond window? Intra window has $f \approx 45$ m, and extra window $f \approx 20$ m.

(iii) Diamond splitters/TFP devices for pump introduction contribution? Insignificant as they are not pressure containment configured and can be ≤ 100 μm thick.

For stretched CPA pulses nonlinear effects will not be important.

Nonlinear self-focusing in CO_2 gas at 10 μm

For simplicity we consider pure CO_2 gas mixes – as the non-linear refractive index of typical gases that may be utilized, as measured, are all in the range of ≈ 10^{-19} cm^2/W. These are mainly monatomic gases such as Kr, Xe, Ar [15,16]. The non-linear refractive index of air (predominantly N_2 and O_2) has been measured at ≈ 9.2 μm to be ≈ 3.0×10^{-19} cm^2/W. [17]

Various values are in the literature for the non-linear refractive index coefficient of CO_2. One extrapolated from 2 μm to 10 μm is in the range of $n_2 \approx 9\times10^{-19}$ cm^2/W-atm and therefore 4.5×10^{-18} cm^2/W at 5 atms. For a nominal PA active length of ≈ 0.4 m (pure CO_2, double passed 0.8 m effective for worst case estimate), and preamp either effectively ≈ 0.9 m or 1.8 m (triple pass of active length ≈ 0.3 to ≈ 0.6 m – latter active length if diluted). The schematics below show some details of the concept:

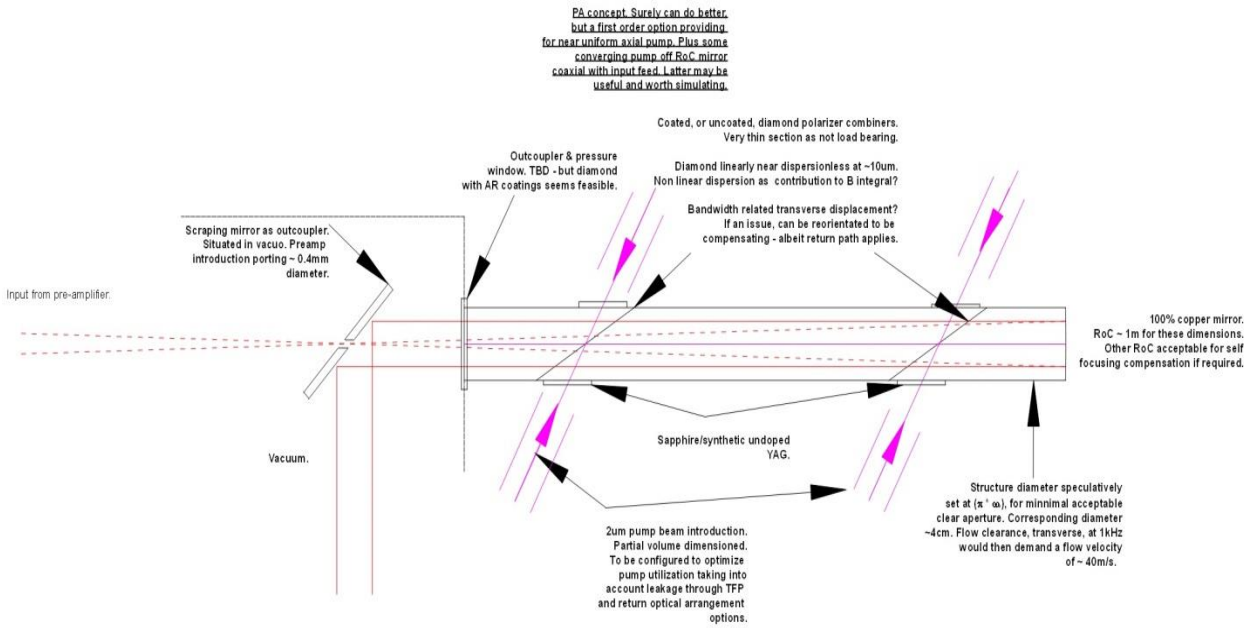

Figure 4: Power amplifier schematic

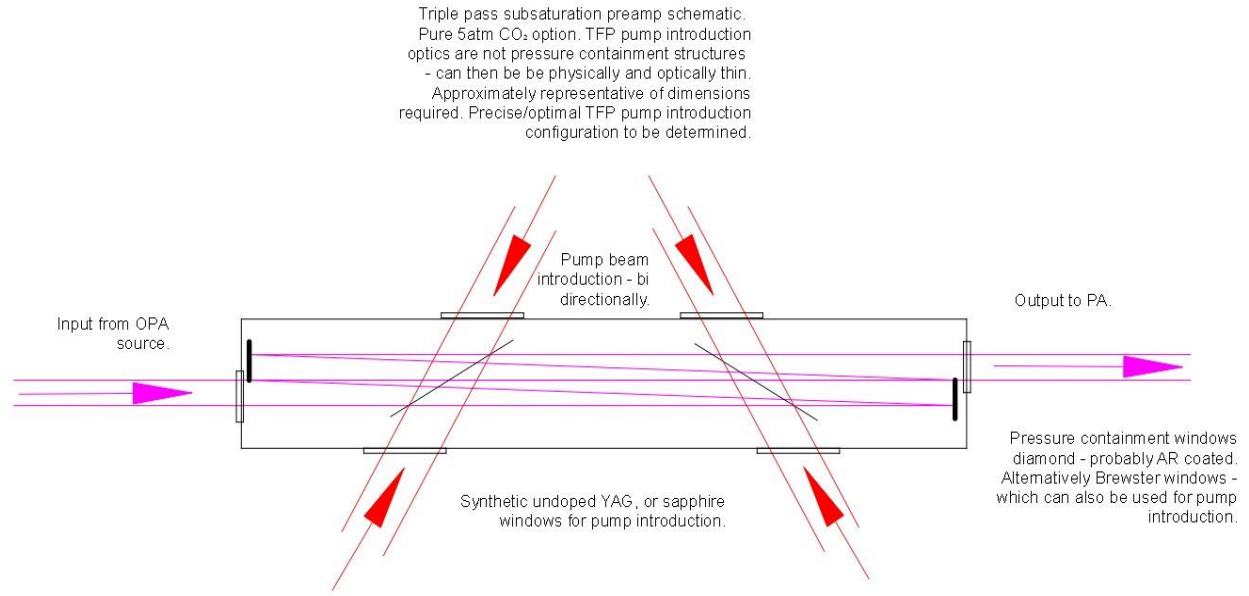

Figure 5: Pre-amplifier schematic

$f \approx 1.1\times10^5(w_0^2/\mathrm{L})$ for 1 TW/cm^2, and $f \approx 0.55\times10^5(w_0^2/\mathrm{L})$ for ≈ 2 TW/cm^2. Corresponding estimates of f for the two respective entrance and exit cases (entrance: 2 mm, 0.8 TW/cm^2 and exit: 12.5 mm, 2 TW/cm^2 exit) for the PA would then be respectively, $f \approx 0.7$ m, and $f \approx 11$ m. These estimates assume L ≈ 0.8 m, with the assumption of the w_0 aperture as constant for the ≈ 0.8 m path (which in terms of the PA concept presented in the layout schematic is not the case). That

constitutes a worst case estimate for the entrance event – and relaxing to a more realistic condition by breaking down into 0.4 m segments, yet still exclusive of the fact that w_0 is not constant axially on these beam paths (thus still a worst case), one gets a revised induced focal length of $f \approx 1.4$ m and $f \approx 22$ m respectively.

Another literature source observes n_2 for CO_2, at ≈1.24 μm, to be $\approx 3\times10^{-18}$ cm^2/W-atm [18]. Thus at 5 atms $\approx 1.5\times10^{-17}$ cm^2/W. Applying the same nominal conditions as in the preceding discussion, one attains revised induced focal lengths of $f \approx 0.2$ m and $f \approx 3.3$ m, respectively. Relaxing as in the preceding to actual 'active' lengths, albeit still ignoring fact that entrant path beam waist is not constant, the expectation is $f \approx 0.4$ m and $f \approx 6.7$ m.

The initial lower bound PA focal length $f \approx 0.7$ m estimate, for constant w_0, applies to an assumption of an effective length of ≈ 0.8 m (or 2×(L ≈ 0.4 m)). This indicates an absolute worst case predicated on the 1st pass. w_0 is in fact dynamically varying over the first 0.4 m before it attains the final exit aperture amplitude waist of ≈ 1.25 cm, and is subsequently conceptually static in return pass in terms of size of the waist. Therefore, the induced focal length will be impacted by the waists actual variation with axial length. A figure of merit numerical estimate for the dynamically varying entrant path focal length yields an effective focal length of $f \approx 7$ m. Therefore, combining the passes (1st and 2nd pass both at ≈ 0.4 m) the net focal length is nominally $f \approx 5$ m, which is not an immediately design concern because an adaptive correction off the intra PA device return mirror is always an option. Given the greater n_2 coefficient possibility reported, the collective net focal length would be roughly $f \approx 1.7$ m, with $f \approx 2$ m for the entrant path. Compensation off the return mirror is possible in principle. The temporally varying radially symmetric negative (linear) lens structure behaviour of the gain medium with axial pumping with a Gaussian radial irradiance distribution as addressed in the AFOSR 2020 interim report (Fig. 9) may also be implemented in mitigation

The evaluation suggests the existence of practical PA and pre Amp physical length limits, for direct USP amplification. It is preferable then to scale the aperture rather than the system component active lengths, and a shorter PA could be implemented. What is reflected in the raw axial dimensioning of the concept CO_2 preamplifier and power amplifier favours CPA function, but can be used for direct USP amplification investigations.

CO_2 pump and pre-amplifier and amplifier response

Optical pumping of CO_2 in the vicinity of ≈ 2 μm, using laser diode pumping with efficient and energy storage capable, solid state lasers, is possible via two paths. The first is direct, and the second indirect. The first was the apparent higher risk option, while the second, a donor-acceptor configuration, seemingly the least risky. The former has a limited quantum efficiency for 10 μm output, of ≈ 20%, while the latter can increase the efficiency to ≈ 40% (which is physically the absolute optimal obtainable for CO_2, supported by a donor-acceptor cross section for relevant near resonant energy exchange of $\approx 2\times10^{-20}$-$3\times10^{-20}$$m^2$). The direct pump path has been successfully demonstrated in Phase 1 (ONR Phase 1 report), resulting in observed optical gain, consistent with

theoretical expectations. The subsequent discussion therefor is restricted to considering this option. Schematically, the direct pump path energy level diagram is as follows.

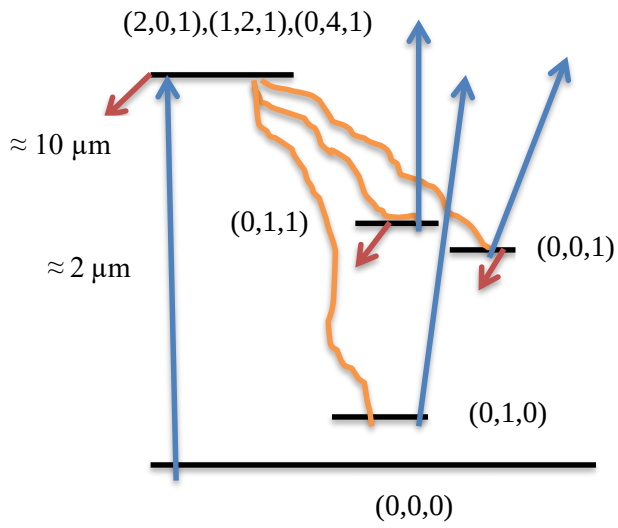

Figure 6: Optical pump to the Fermi resonant (2,0,1), (1,2,1), (0,4,1) levels (pump band). Subsequent near resonant V↔V exchange processes resulting in population of metastable (0,1,1) and (0,0,1) levels. Population transfer into the (0,1,0) level (plus peripherally the (1,0,0) and (0,2,0) levels for example).

Spectrally, concordant to pump, secondary pump transitions out of identified levels. Consequently, CO_2 pump does not significantly saturate.

Most resultant excited levels generally contribute to net gain distribution and 10 μm lasing at pressure.

With regard to CO_2 response within regular band and sequence bands, the V→V-1,R,T relaxation coefficient of the regular band is ≈ 4 μs-atm. This time constant is known to decrease with increasing v_3, thereby increasing rate of loss of vibrational energy to rotational and translational degrees of freedom. Less well established are the forward (k_f) and backward rate (k_b) coefficients of the CO_2 anharmonic vibrational energy transfer process:

$$CO_2(0,0,v) + CO_2(0,0,v) \leftrightarrow CO_2(0,0,v+1) + CO_2(0,0,v-1)$$
$$k_f \rightarrow$$
$$k_b \leftarrow$$

and a number of similar processes

$$CO_2(0,0,v+1) + CO_2(0,0,v) \leftrightarrow CO_2(0,0,v+2) + CO_2(0,0,v-1)$$

Estimates for k_f have been extracted from two publications, existing Phase 1 data (ONR Phase 1 report), and two specified literature sources, in its simplest process form for $-2\times k_f \times n_{(001)} \times n_{(001)}$ [19-22]. Extracted k_f estimates depend on the observed sequential dual time constant decay process observable in the papers of RC Auyeung [20], D Tovey [19], and the identified Phase 1 (ONR Phase 1 report) results. In the case of the latter, profiled on the Gaussian pumped radially distributed peak gain, not the spatial average, as the process is principally population driven. Simplistically, for the anharmonic V↔V exchange process, the forward process related decay will arrest as it enters detail balance with the backward process, with V↔V exchange driven population of the (0,0,2) sequence band. The condition being $k_f \left(\frac{n_{(001)}}{n_{(000)}}\right) \approx k_b \left(\frac{n_{(002)}}{n_{(001)}}\right)$, and threshold for transition out of anharmonic process dominance is level population number density

dependent. This phenomenology is observable in the specified literature sources utilized in estimates. The respective values are: $\approx 3.4\times10^{-18}$ m^3/s; $\approx 3.7\times10^{-18}$ m^3/s; $\approx 1.6\times10^{-18}$ m^3/s; $\approx 4.8\times10^{-17}$ m^3/s; $\approx 0.4\times10^{-18}$ m^3/s. These values are not inconsistent with known anharmonic V↔V exchange process coefficients for the hydrogen halides, and other gases, within a two order of magnitude range. A range, at raised partial pressure of CO_2, for supportable small signal gains, resulting in rates complementary to the objectives of this technology proposal. That given, to the upper end of the k_f value range, the general features and relevance presented in the plots below remain, other than for a reduction in the timescale of the projected anharmonic process identifiable structure timescale. The k_f value employed in the plots is an average of those extracted from the first two publications identified, and the Phase 1 (ONR Phase 1 report) data.

An estimate of the k_b return process, $2\times kb\times n_{(002)}\times n_{(000)}$, rate coefficient value for CO_2 can be estimated subject to an assumption that the basic anharmonic V↔V exchange process should sustain thermal equilibrium under normal conditions.

$$\frac{k_b}{k_f} \approx e^{-\frac{\left(\Delta E_{(001)}-\Delta E_{(002)}\right)}{kT}} \approx 0.85$$

This for the specific Phase 1 (ONR Phase 1 report) isotopologue employed.

We utilize the preceding to develop an indication of aspects of high partial pressure, CO_2, function, other than those already identified, that are potentially relevant. Regular band ((0,0,1)), and regular band plus sequence band ((0,0,2)), population response subject to both the anharmonic V↔V up conversion process and standard V→V-1,R,T relaxation is represented. In each case evaluations are executed for pure CO_2 and 1:1 CO_2:Xe dilution. Induced initial inversions are matched to represent similar gain situations for the dilute and undiluted cases. Subsequent simulated behaviour is plotted. In most sequence band situations in CO_2, and therefore sources of potential hot band lasing transitions analogous to the standard (0,0,1)→(1,0,0) or (0,0,1)→(0,2,0) transitions, albeit red shifted typically, there is considerable pressure broadened assisted overlapping of most of the resultant gain distributions. The combination of regular and (0,0,2) sequence band population can then be considered to be an indicator of collective gain response. However, anharmonic up conversion pumping of for example the (0,0,2) sequence band is not a system loss energy process, but will be an energy loss channel if significant population is moved into the (0,0,2), (0,0,3) and above sequence bands, and on lasing interaction event, these cannot cascade down sufficiently rapidly to yield multiple sequential interactions within the necessary timescale to enable efficient extraction of the multiple quanta therein invested. In the following evaluations the pump is assumed to be an instantaneous net population transfer into the (0,0,1) level.

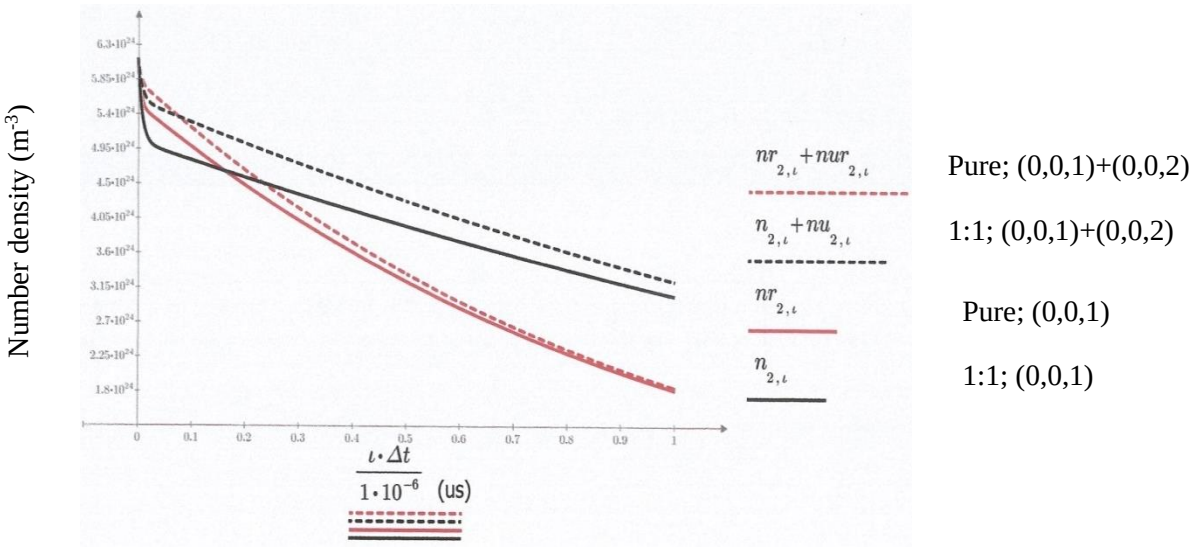

Figure 7: Pure CO_2, net 5% inversion. 1:1 dilute mix, 10% CO_2 inversion. 296 K ambient. 5 atm.

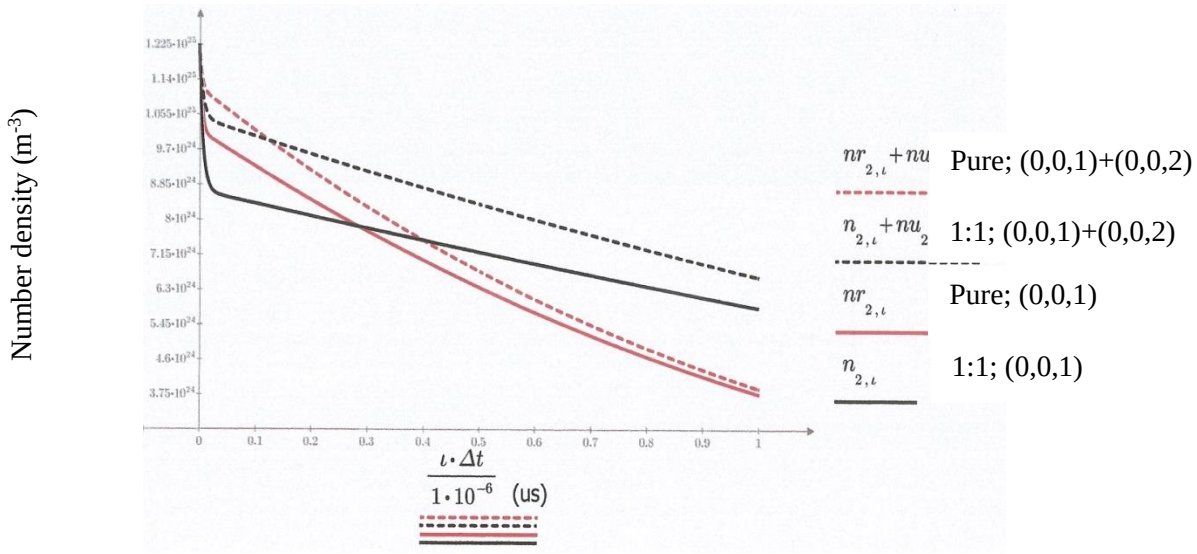

Figure 8: Pure CO_2, net 10% inversion. 1:1 dilute mix, 20% CO_2 inversion. 296 K ambient. 5 atm.

It is apparent that a greater CO_2 partial pressure raises the population density threshold at which the anharmonic up conversion process becomes dominant, for similar net gas pressure, and a desired common initial inversion, and therefore small signal gain. The greater partial pressure option then similarly displays lesser anharmonic process related population redistribution associated small signal gain decay. Equally, be gain associated with the regular band, or a combination of regular band and sequence band populations, for timescales applicable to amplifier access of less than 100 ns, the pure and thus high partial pressure gas mix is favourable. The initial up conversion process induced gain decrement is minimized for the pure CO_2 gas mix, as previously identified. In the case of the net 5% inversion driven pump and pure CO_2, the vibrational temperature is ≈ 1100 K immediately post the anharmonic process, and for the corresponding dilute case,

of 10% net inversion for similar gain specification, the vibrational temperature attained ≈ 1450 K. Therefore, the objective of attaining the desired gain, for a tolerable T_3 as discussed in the introduction, is better supported at high CO_2 partial pressure. Increasing the dilution of the CO_2 in the gas mix will rapidly increase T_3 for a given small signal gain. 5% inversion for pure CO_2 corresponds to a small signal gain of ≈ 10 m^{-1}. A corresponding 10% inversion for pure CO_2 gas mix would correspond to a small signal gain of ≈ 20 m^{-1}, and T_3 ≈ 1450 K. In the case of the corresponding dilute case of 20% net pump for a similar gain, the vibrational temperature would reach ≈ 2070 K. There is clearly a transition from a modest anharmonic up conversion influence, to something that is no longer insignificant in stepping between these two pumped population density points.

Pulsed interaction saturation energy for CO_2 narrowband, and even extended to CO_2 broadband, albeit inherently for a rate approach, not coherent response is relevant.

Conventionally, narrow band, inhomogenously broadened, strictly 2 level:

$$E_s \approx \frac{h\nu}{2Z\sigma},$$

which for 10 μm, 5 atm pure CO_2, $Z \approx 0.07$ and $Z\sigma$ equal to the bulk emission section, ≈ 0.5 J/cm^2.

$$\sigma \approx \frac{A_e\lambda^2}{4\pi^2\beta P}\zeta,$$

where ζ is the ro-vibrational transition cross influence enhancement factor at 5 atms.

From the numerical simulations applied, $E_s \approx 0.54$ J/cm^2 at 5 atms, and approximately 70% of linear amplifier response is attained at ≈ 0.65 J/cm^2.

A broad band adaption of the forgoing, would be to consider the gain medium in its entirety as homogenously broadened, in which case $Z \approx 1$, and σ is then modified in terms of the homogenous gain medium structure bandwidth, which for a single molecular isotopologue P branch structure is ≈ 600 GHz FWHM, still considering a 2 level approximation, resulting in $E_s \approx 0.7$ J/cm^2.

Of interest, as a figure of merit, is the pump fluence (pulsed pump, J/cm^2) required to drive the identified percentage inversion for a small signal gain of ≈ 10 m^{-1}, or alternatively the net population projected into the regular and/or regular plus sequence bands identified. This for the CO_2 pump bands for the direct pump path option, matches the Tm:YAG spectral capability as the DPSS front end.

$$E_p \approx \frac{n_{inversion}h\nu_p}{(1-e^{-1})}l_p,$$

where $h\nu_p$ = pump photon energy, and l_p = pump absorption scale length. The latter varies, for 626-636 CO_2, for example, at 5 atms, for a spectrally accessible pump transition corresponding to the identified DPSS front end, from 10-15 cm, ≈ 9-14 J/cm^2.

For a pump pulse of ≈ 100 ns FWHM, the forgoing is attainable and sustainable, and typically not constrained by probable system optics LIDT [23-26]. Selected references address the USP regime, given the possible consideration of direct USP amplification. It is also the apparent from the preceding, that for the now established pump fluence range, that dilution of CO_2 to a reduced partial pressure will not change the resultant percentage inversion driven ($n_{inversion}/n_g$) as $l_p \approx (\sigma_p \times n_g)^{-1}$. Thus T_3 largely retained, at the expense of a near proportional extension in pump scale length.

Note that by imposition of an appropriate pump profile the Gaussian nature of the amplified beam may be preserved through the device. But there is interest in retaining not just the radial distribution, but the spectral distribution as well. Similarly then, in pre saturation, with a top hat gain profile, the bandwidth of the pulse may be preserved, as is the radial irradiance distribution. In the case of the PA, in contrast, for near to above saturation function, with a top hat pump profile, the pulse bandwidth may be preserved or increase depending on implementation. This suggests, that retaining a near Gaussian irradiance profile in PA transit by choice of an appropriate pump radial profile, a pump profile may exist that represents an optimal compromise between maintaining pulse bandwidth and a Gaussian irradiance profile, while optimizing system efficiency. The latter focus on optimizing efficiency as top hat pumped pre-saturation function sacrifices energy. The optimal case is then to configure a design such that the PA functions in or near saturation, with an optimal partial volume pump.

CO_2 Pre-amplifier

A strictly 2-level simulation is applied for a triple pass pre-amplifier. An active length of ≈ 0.9 m, for a 0.3 m long pre-amplifier, of pure CO_2 at ≈ 5 atms with small signal gain of ≈ 10 m^{-1}, at a wavelength of 10.6 μm and an amplitude waist of $w_0 \approx 3$ mm. The corresponding Rayleigh range is ≈ 2.7 m, which is a good match for the active length if the waist is located at the midpoint of the amplifier active length. An input pulse from an OPA with an energy of 14 μJ is assumed and a top hat pump profile emulated by a radially truncated but broad pump Gaussian with waist of $w_{0p} \approx 20$ mm. Truncation provides a representation of partial volume pumping.

Note the pre-amplifier is, by its system role, inherently energy sacrificial. That is, it is not intended to be wall plug efficient. Conveniently, it is not comparably the energy consumer of the PA component of the CO_2 optically pumped amplification component of the system.

- Output pulse energy 49 mJ with 0.33 J/cm^2 peak fluence.
- Pre-amplifier optical gain ≈ 3,400.
- Pump energy required ≈ 30 J.

- Pre amplifier efficiency for 10.6 μm using 2 μm direct pumping of CO_2 is $\eta \approx 0.16\%$. *With successful implementation of indirect pumping, the efficiency is anticipated to double to* $\eta \approx 0.3\%$*, with 15 J pump.*

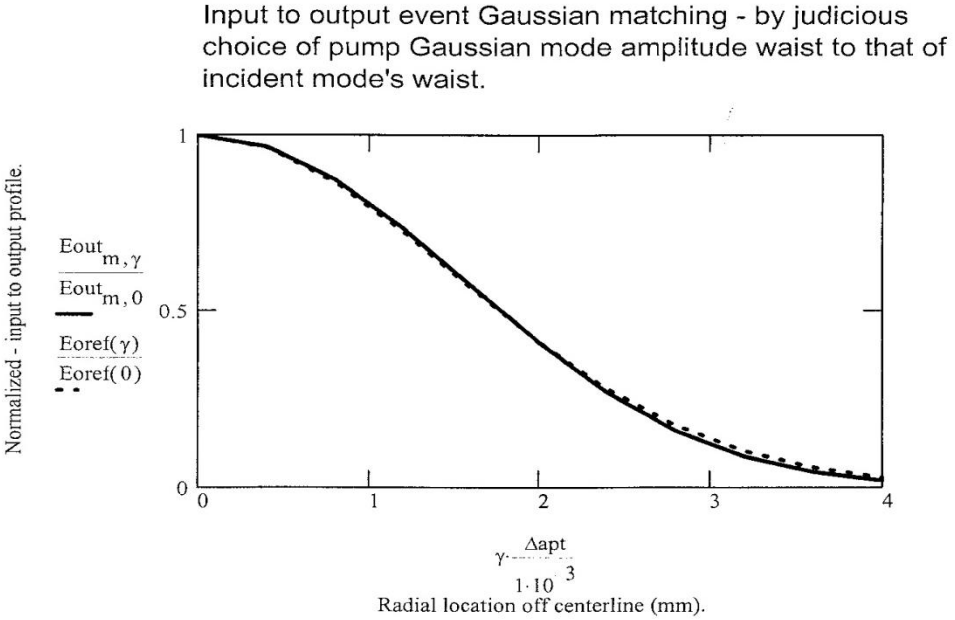

Figure 9: Pre-amplifier. Solid line: normalized irradiance of output profile. Dashed line: normalized irradiance of input profile.

CO_2 power amplifier

As with the pre-amplifier, a strictly 2 level simulation is applied for a double passed amplifier with an active length of ≈ 0.8 m and a 0.4 m long power amplifier, using 5 atms of pure CO_2, giving a small signal gain of 10 m^{-1} at 10.6 μm. The waist is variable on the 1st pass, and is $w_0 \approx$ 1.25 cm for output path. The input pulse, from the pre-amplifier is ≈ 50 mJ. The pump profile is Gaussian, with a waist greater than the 10.6 μm interacting pulse.

Note the power amplifier is near or at saturation, and usefully partial volume pumped as indicated by the pump Gaussian profile's relation to that of the interacting 10.6 μm field. An energy efficient application. This serves to optimise system wall plug efficiency. The power amp is the primary energy consuming component of the system.

- First pass energy (net) yield ≈ 1.05 J, or ≈ 0.43 J/cm^2 peak fluence.
- Second pass out coupled (net) energy ≈ 5.3 J, or ≈ 2.2 J/cm^2 peak fluence.
- Pump energy required ≈ 90 J.
- Power amplifier optical gain ≈ 106.

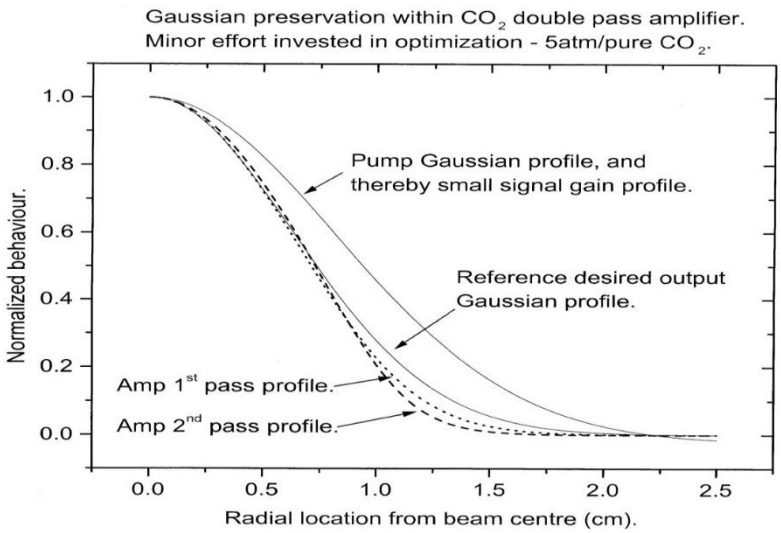

Figure 10: CO_2 Power amplifier double passed. Solid lines = normalized pump and input reference profiles. Dashed lines = normalized post 1st and 2nd pass irradiance of profiles.

Power amplifier efficiency at 10.6 μm, for ≈ 2 μm direct CO_2 pumping, is $\eta \approx 6\%$. This for a strictly 2 level model, with the entire rotational structure accessed. The time constants of (1,0,0)↔ (0,2,0) and (1,0,0)+(0,2,0)↔(0,1,0) V↔V level to level relaxation processes are relevant. They range temporally from near gas kinetic timescales to nanosecond scale for 5 atms of CO_2. Consequently, for ps to 10s ps events, they are 'frozen' out of any interaction. However, for CPA, or for multi-passes through same volume geometries, with suitable delays between passes, they will contribute. A 1 m of optical path length gives ≈ 3 ns delay.

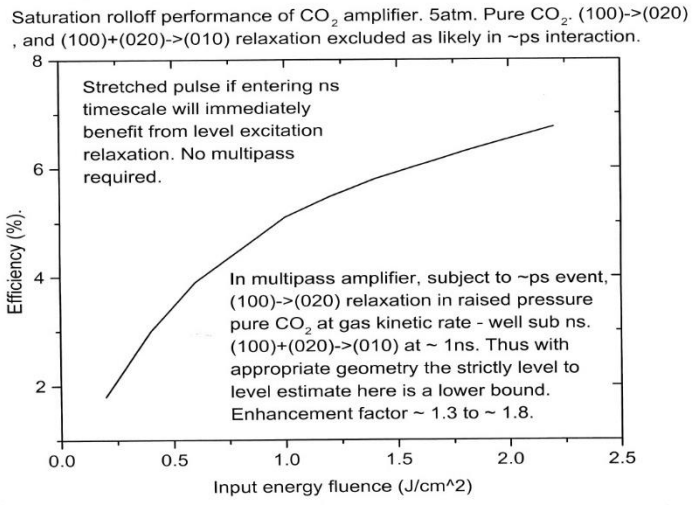

Figure 11: Efficiency as a function of input fluence of CO_2 power amplifier concept.

A CPA or multi-pass implementation for reasons related to the then feasible level to level energy exchange, using a directly pumped PA is expected to attain a conversion efficiency in the

range of η = 7.8-10.8%, for a 70-50 J pump. For indirect pumping the PA conversion efficiency is anticipated to double to η = 15.6-22% for 35-25 J pumps. These estimates were predicated on a limited peak interacting fluence, constrained by LIDT and non-linear effects, yet attempting to attain a level of gain saturation within the CO_2 PA. CPA allows the interacting fluence across the spatial Gaussian transverse profile to be enhanced, raising system efficiency. The enhancement can approach 40%, resulting in a conversion attaining in principle something in the range of η = 11-15% for direct pumping, and 21-31% for indirect pumping.

Associated CO_2 OPML DPSS system Tm:YAG front end elements.

The pump is the heart of an OPML system. The preceding considerations provided the DPSS specifications for the concept CO_2 OPML DPSS system. The DPSS parameters such as pulse energy are broadly established. The DPSS system must be spectrally matched to the CO_2 pump bands, which are in the range 2-2.05 μm. A number of options exist. Tandem pumped optical parametric amplifiers (OPAs) based on 1 μm high power lasers are an option. However, OPAs are inefficient, complex, not readily scalable, and not very reliable. Alternative options are the transition metal doped II-VI semiconductors, ZnSe and ZnS, but they suffer from very strong thermal lensing, and low optical damage thresholds. To exploit the CO_2 (0,0,0)→(0,0,1) fundamental as a pump transition, a Fe^{2+}:ZnSe system is inherently inefficient as a front end because the DPSS front is Er:host, and the OPML front end then is a tandem pumped system requiring typically a cryostat for the Fe^{2+}:ZnSe element. Staged OPAs in near degenerate function, with a tandem plus tandem system attaining approximately 4 μm, pumped around 1 μm, are also possible, but become a very complicated multi-element system. In addition, because the CO_2 (0,0,0)→(0,0,1) transition is very strong, spectral detuning or significant gas mix dilution is a prerequisite for useful pump scale lengths at around 4 μm. In the event then of a desire to utilize an arbitrary CO_2 multi-isotopologue gas mix, the pump band spectral range presents a complication.

An alternative route is to use dopant materials with transitions that directly emit at the desired wavelengths. This is a simple, robust and efficient engineering approach that does not require much maintenance. Suitable materials are trivalent thulium or holmium, both of which have excellent optical to optical conversion efficiencies within their host media. Thulium is suitable for direct laser diode pumping with affordable, commercially available high power arrays. Holmium is not. This suggests that Tm:YAG and Tm:host media are well suited to scaling to significant pulse energies.

The gain medium considered for this report is Tm:YAG as it has a long-excited level lifetime that lends itself to laser-diode pumping using affordable diode arrays. The dopant Thulium has a significantly smaller thermal population in its lasing terminal energy levels than holmium, and is thus favourable from a laser threshold and extraction efficiency standpoint in principle. It has a smaller emission cross section than holmium, which results in a larger saturation energy for pulsed operation. But it is then energy storage favourable and presents with an acceptable gain-length

product for useful active medium lengths, without risking amplification of spontaneous emission (ASE) or a tendency for parasitic oscillation. It lases within the spectral band of interest, and if tuning is required this can be achieved using a sapphire prism arrangement intracavity. In regards the saturation energy feature, this is accessible to an optical engineering solution for both the DPSS amplifiers and oscillators required, this enabled in part by the LIDT of the selected host material, both in bulk and surface [27-29]. It benefits from modest cooling [30], yet also operates at cryogenic liquid N_2 temperatures, though this makes any system more complex. The host medium, YAG is suitable from a thermal conductivity, thermo-optic and thermal expansion coefficient change standpoint, if cooled [31].

Consideration of Tm:YAG subject to the forgoing and other related features, leads into the following conclusion set:

Design for the lowest dopant concentration (atm. %) without compromising the efficiency of the 2 for 1 pump cross relaxation process within Tm^{3+} as laser diode pumped in the range of 760-800 nm ($^3H_4+^3H_6 \rightarrow 2\,^3F_4$). Up conversion $2^3F_4 \rightarrow {}^3H_6+{}^3H_5$ exists, an undesired loss process that is to some degree dopant concentration dependent.

This optimises efficiency because it reduces the pump energy required to attain threshold inversion. Certainly beneficial at low repetition rates, yet also favourable for higher repetition rates.

Modest or cryogenic cooling is viable and possibly advantageous. It bootstraps the preceding points, predicated on dopant concentration selection, by leveraging thermal Boltzmann population redistribution, within the lasing and terminal level manifolds. This reduces the saturation energy of the system, reduces pump energy required to attain threshold, and typically increases the pump deposition per unit volume for a given spectrally located pump and medium dopant concentration. Up conversion is favourably influenced by cooling.

The preceding three points move the system towards 4 level behaviour.

Long pulse operation relaxes LIDT thresholds, in addition to allowing fluences at or in excess of saturation. Long pulse operation is also desirable as it is complementary to the pump CO_2 $V \leftrightarrow V$ energy exchange rate kinetics. Long pulses from a DPSS system also facilitates relaxation within each level multiplet of Stark sublevels.

Meeting the required pump absorption for a given configuration is possible by spectrally tuning laser diodes, cooling, utilizing optical engineering, and increasing dopant concentration.

Tm:YAG pump

Up conversion is an undesirable loss of the 2 for 1 pump cross relaxation process. It has been primarily associated with the ${}^3F_4+{}^3F_4 \rightarrow {}^3H_5+{}^3H_6$ process, with subsequently high branching ratio, ${}^3H_5$ relaxation into ${}^3F_4$ [32,33]. Therefore, it contributes to thermal loading and loss of efficiency during pumping. Limiting approximate achievable excited level population $n({}^3F_4)$ can be crudely represented as a function of the upconversion and the deliverable pump irradiance.

$$\frac{\sigma_p n_g I_p}{h\nu_p}\xi \approx k_{uc} n({}^3F_4)^2,$$

where $\xi = 2$ for 1 efficiency factor ≈ 1.8-1.9, σ_p is the bulk pump transition cross section (detuned in this case to yield useful pump absorption scale length of 1cm at 4 atomic %), pump irradiance $I_p \approx 4$ kW/cm^2, $h\nu_p = 790$ nm pump photon energy, k_{uc} is the up conversion coefficient ($3.49\times10^{-3}\times T - 2.9\times10^{-2}$)$\times 1.8\times10^{-18}$ cm^3/s.

$$n({}^3F_4) \approx 1.3\times10^{20}\,\mathrm{cm}^{-3}.$$

Approximate inversion, correcting for possible room temperature lasing terminal level population, yields ≈ 1×10^{20} cm^{-3}. Potential volumetric extraction is limited to 9 J/cm^3 at 2 μm, for a corresponding small signal gain of 20 %/cm. The temperature dependence of k_{uc} at 200 K positions it at ≈ 67 % of its room temperature value, and at 77 K it is 24 %. These preliminary predictions are useful performance parameter guides in practice, albeit limiting. The pumping process merits a more detailed behavioural evaluation.

A detailed pump process simulation has been established, and the following is a compilation of the relevant predictions.

For 4 atomic % Tm in YAG, the laser diode pump fluences are 4 kW/cm^2 and 8 kW/cm^2, for room temperature and 200 K. The pump is assumed sustained for the duration of the evaluation. In each case, three progressively more detailed simulations are applied.

The population estimate for ≈ 4 kW/cm^2 from the crude analytical term did not incorporate pump transition saturation as a limiting factor. Of interest is the increment in achievable ${}^3F_4$ level population density presenting with modest cooling for identical pump irradiances, which is attributable, in part, to the enhanced pump power per unit volume applied because of Boltzmann population redistribution, and temperature modifications in k_{uc}. Additionally, the reduction in terminal laser level population for the modest temperature reduction of ≈ 90 K is significant.

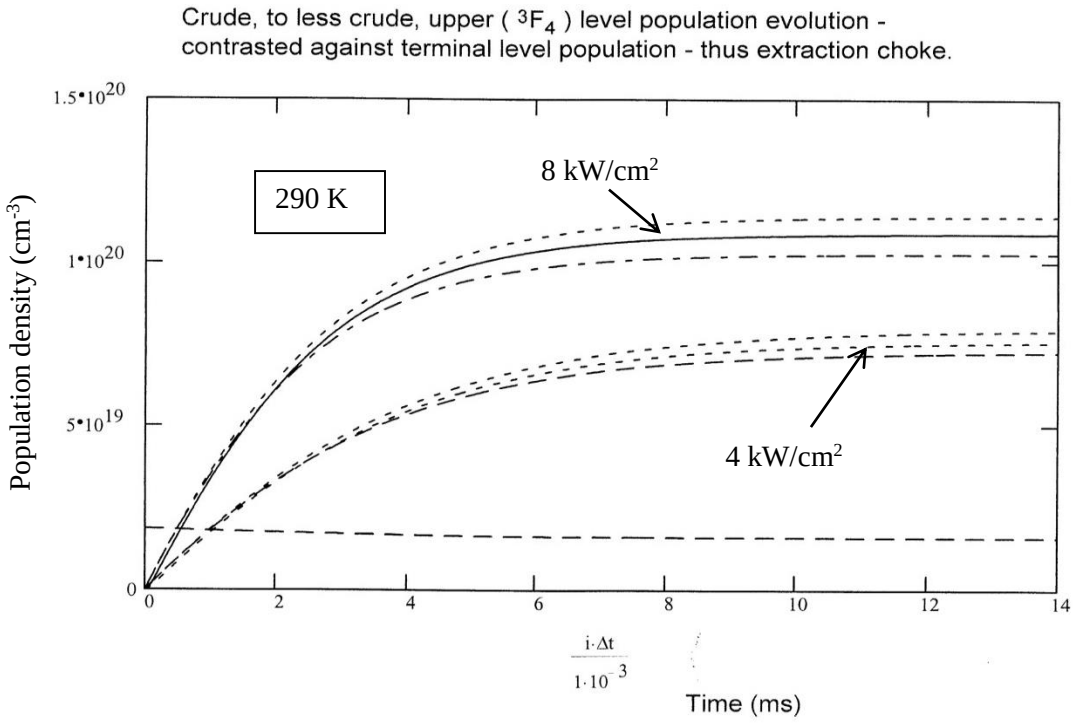

Figure 12 Population evolution at 290K.

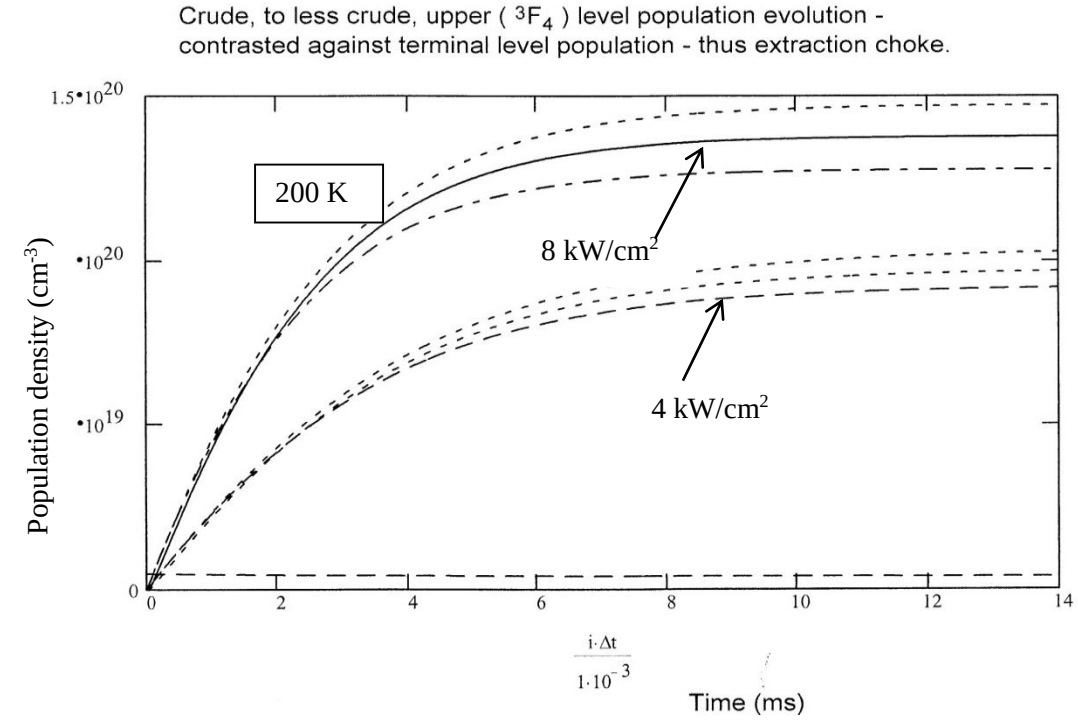

Figure 13 Population evolution at 200K.

The temporal response of the pump process is of interest. Specifically the pump as qualified by the nominal terminal lasing thermally attributable population, thus threshold investiture required. Thus a representation of the dynamically varying extractable energy storage relative to net pump applied, modified by loss processes, and thus an effective pump efficiency.

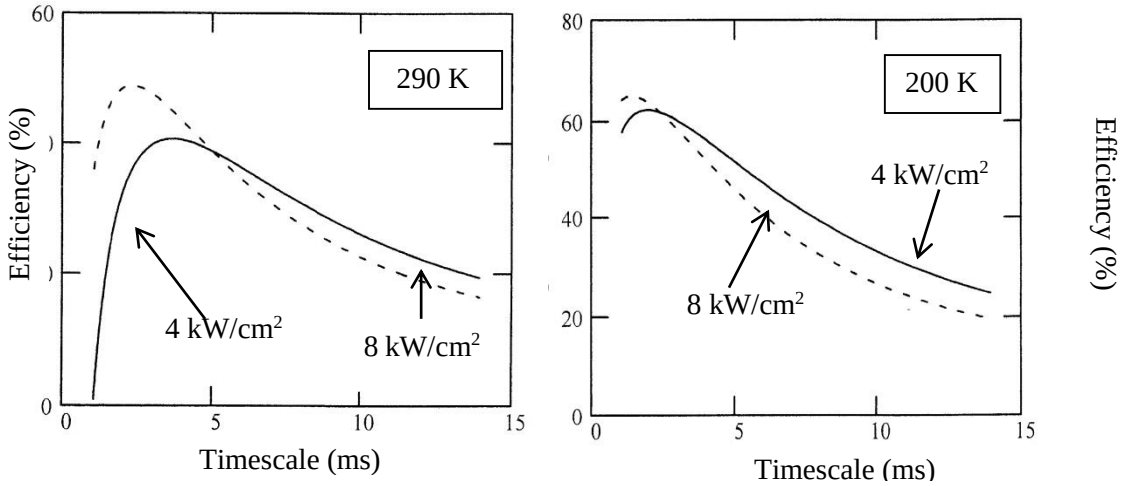

Figure 14. Pumping efficiency

There is in both temperature, and to an extent pump irradiance cases, an identifiable optimal pump event duration. As the pump irradiance increases and the temperature decreases it converges on the theoretical limit of 79% for a 790 nm pump. In the 290 K case, the optimal pump duration is in the range of 2.5-4.0 ms, and for 200 K, it is found in the range of 1.5-2.5 ms. To optimize performance and minimize medium heating, for an isolated pulse, or a CW pumped repetition rated system, this applies for the isolated pump pulse or generally as the period of an optically switched repetition rated system. A limiting pump efficiency of $\eta \approx 65\%$ is attainable at 200 K. This is subject to the onset of pump saturation, onset of significant up-conversion, and thermal differences in population distribution.

Comparing the optimal time constants with the preceding associated $^3F_4$ population temporal behaviour curves and terminal level condition, possible peak volumetric extractions and small signal gains of 4-5.2 J/cm^3 at 8-10.4 %/cm are indicated at 290 K for the two pump conditions. At 200 K possible peak volumetric extractions and small signal gains of 5.3-6.0 J/cm^3 at 10.8-12.0 %/cm are indicated respectively. These all for a pump efficiency factor increasing from 40-65%. There is no prohibition on pumping on timescales beyond the optimal, but this will deliver a diminishing return for the energy deposited.

Of direct relevance to the pumping performance is the up-conversion modified $^3F_4$ level lifetime. This is for the 200 K case, as it is viewed as most advantageous, and is technically practical.

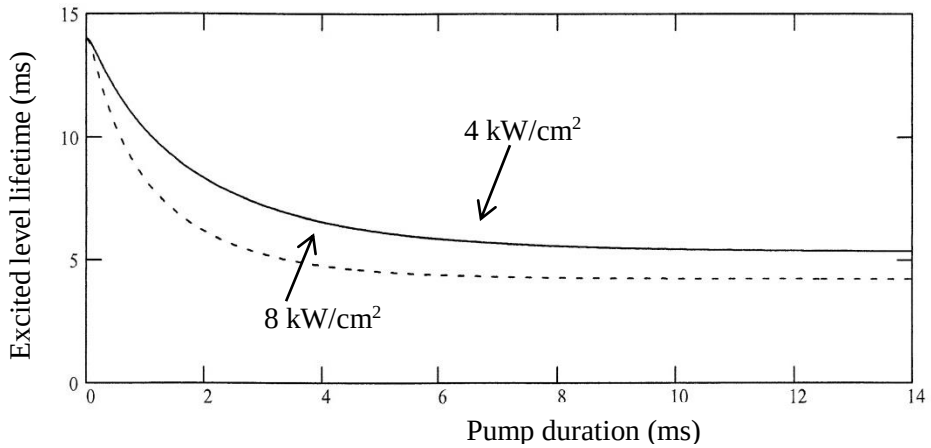

Figure 15. Evolution of $^3F_4$ level lifetime during pump event. Goal is to accomplish pump event within dynamic variation time.

Inspection of the preceding pump efficiency profiles is indeed consistent with the stated goal of restricting pump event to within dynamic variation time, and therefor on average the greatest lifetime, resulting in optimal behaviour.

Further considerations lending weight to the conclusion that function at ≈ 200 K represents a desirable, never mind engineering wise attainable, operating point for the Tm:YAG DPSS front end of the proposed system are respectively.

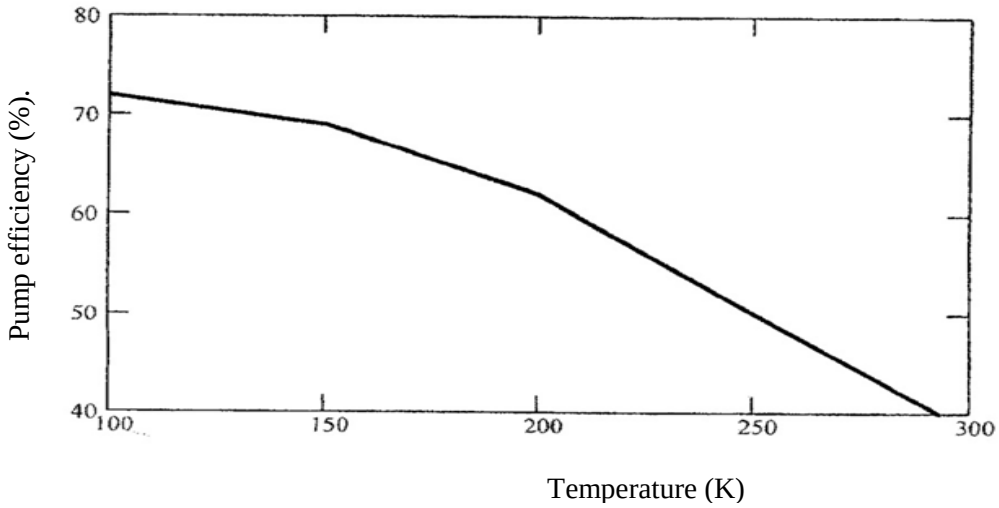

Figure 16: Optimal qualified pump efficiency as function of medium temperature. 4 atm. % Tm:YAG. Pump irradiance 4 kW/cm^2.

Apparently a modest temperature reduction of ≈ 90 K results in a better than 25% enhancement in related performance. Subsequent performance increments roll off with decreasing temperature.

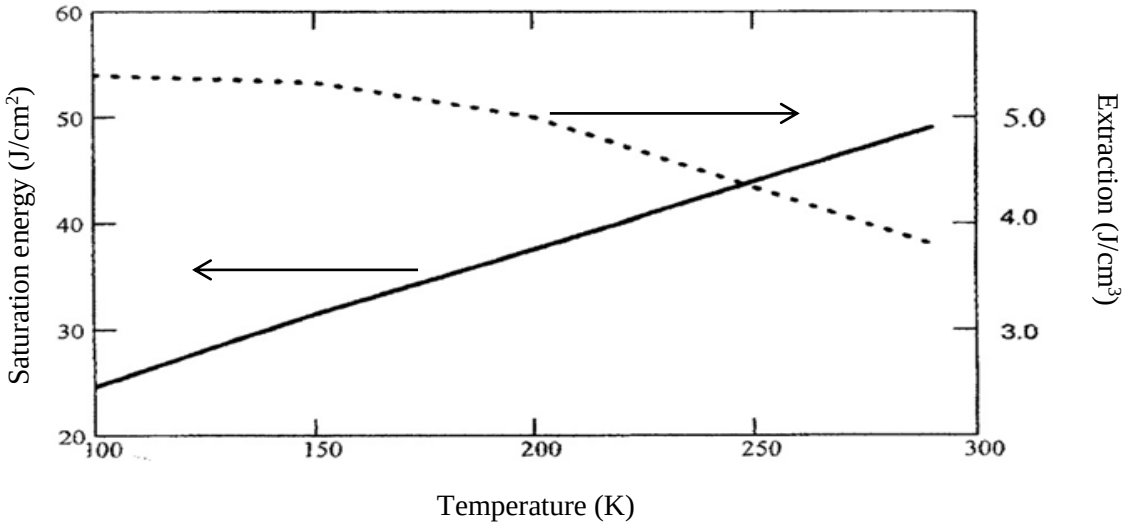

Figure 17: Pulsed saturation energy in Tm:YAG, 4 atomic %, and peak volumetric extraction, pumped at 4 kW/cm^2, feasible as function of temperature.

Figure 17 shows that the predominant advantage in peak volumetric extraction, and thus possible system extraction, occurs for a modest temperature reduction of 90 K. The reduction in saturation energy to less than 40 J/cm^2 at 200 K is equally of value. This value presents given the possible engineering of device configurations where the saturation energy is attained in gain media for long laser pulses, while maintaining the interaction surface and bulk material LIDT within their design specifications. Note that these results derive predominantly from population thermal redistribution. Examination of the publication of J Korner et al., [30] compared with our results, suggests that there may additionally be line narrowing of the transitions in Tm:YAG, which could result in a more substantial reduction in saturation energy by the increase in emission cross section with decreasing temperature. The results suggest that 200 K is a good operating point for Tm:YAG.

Tm:YAG oscillator

A CO_2 pre-amplifier requires a top hat pump profile, while a CO_2 power amplifier MOPA driver requires a Gaussian output profile oscillator front end.

For 200 K, and a required 30 J per pulse output for a pulse FWHM of ≈100 ns, at an intracavity fluence limit of 20 J/cm^2 to maintain comfortable function within YAG surface and bulk LIDT, plus possible AR and mirror coating LIDTs [27,28,34,35], with cavity configured such that cavity mode is double pass and overlaid within pumped active volume of gain medium resulting in an in medium fluence of 40 J/cm^2, and a Brewster surface fluence of 35 J/cm^2, on that element.

A cavity gain medium active length condition for $E_{intra} \approx 20$ J/cm^2 intracavity as a tolerable limit, subject to medium properties such as emission cross section, pump condition in the form of

small signal gain, lasing photon energy, cavity mirrors and engineered beam folding multiplicity in gain medium is of the form:

$$L_a \approx \frac{\sigma(1 - R_1R_2)E_{lidt}}{\alpha h v_l} - \frac{Ln(R_1R_2)}{2\alpha\xi}.$$

It is employed to establish an approximate initial parameter space for detailed simulations, consistent with the specified goal.

Figure 18 shows a schematic of a concept oscillator layout, meeting some objectives.

2 dimensional schematic of preliminary oscillator concept. Restricted to the plane all optics are P polarization incident, but the forward and backward beams transiting the gain medium within this simple view do not overlay optimally, unless the gain medium is sufficiently thin.In practice the beam overlap within the gain medium may be optimized , while retaining Brewster incidence conditions on gain medium (nominally a disc), if the beam path structures of the schematic, viewed as contained in two planes currently within page, each the beam path bottom to top, left to right and right to left respectively, are rotated within their planes about axis a/a clockwise and anti-clockwise respectively - to bring them as closely coincident as practical. The two intracavity sequential folding mirrors move with the related planes. They form intracavity a possible arrangement to appropriately configure the beam's polarization between the two Brewster facets. Fluence on all cavity mirrors, or Q switch, ~ 20J/cm^2 or less depending on AOI to incident beam.

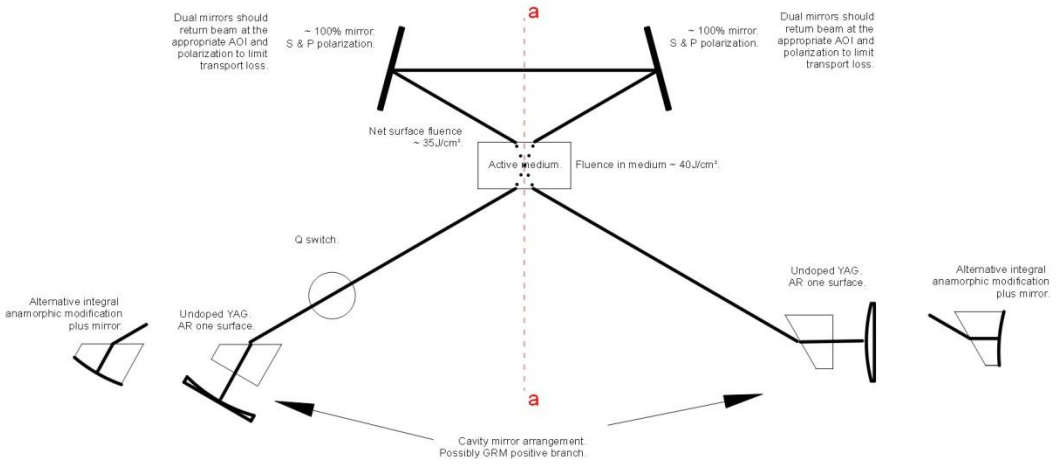

Figure 18: Oscillator layout.

The arrangement of active medium, free space beam paths, and intra-cavity folding mirrors, appears with more clarity in the following image, with the adjacent image showing the volumetric overlap within the gain medium for beams of appropriate cross sectional profile:

Simulation results for a device, of pumped inversion ≈ 10% (small signal gain ≈ 17 m^{-1}), at ≈ 200 K, physical gain medium active length ≈ 1.9 cm (effective in cavity ≈ 3.8 cm as double pass), ≈ 40% out coupling, cavity length ≈ 1.5 m and suitable active aperture yields ≈ 30 J in ≈

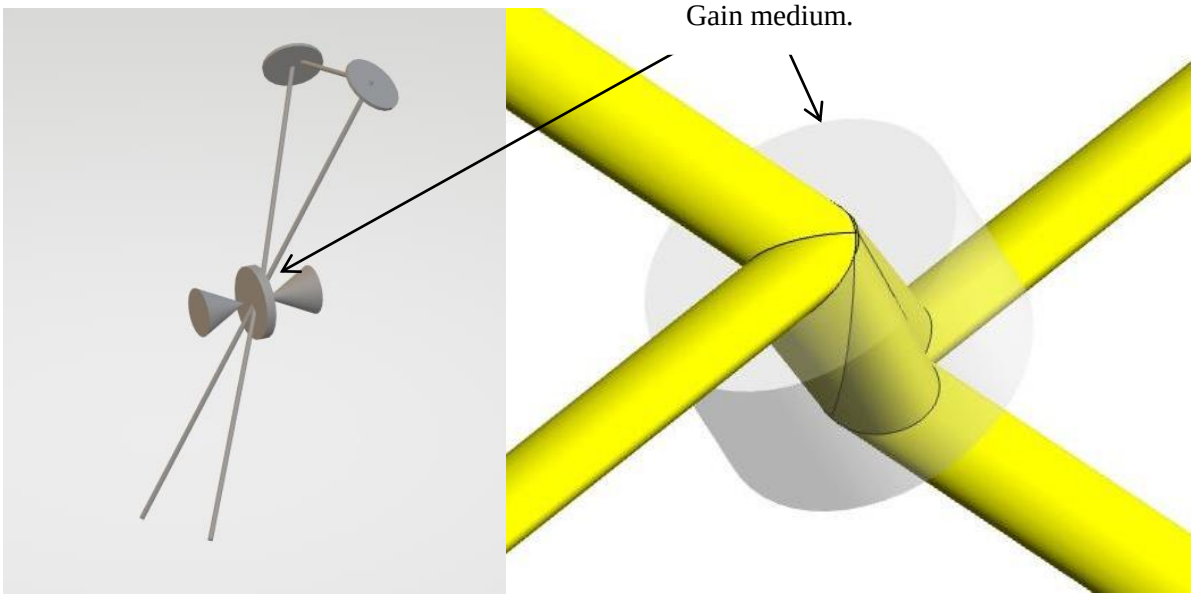

Figure 19: Detailed pumping arrangement. The cone structures denote bi-directional optical pump access to gain medium for laser diodes.

100 ns FWHM. The intracavity folding mirrors offer reflectances of 99.7-99.9% for P and S polarizations respectively, and the attributable round trip cavity loss will be ≈ 1%, which is of limited relevance versus out coupling.

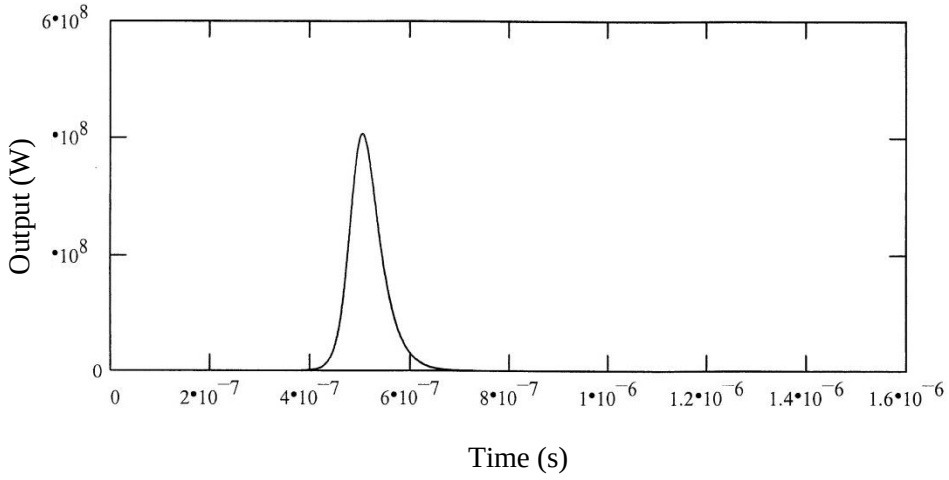

Figure 20. Oscillator output pulse profile (W).

Volumetric extraction ≈ 4.3 J/cm^3, medium optical to optical conversion efficiency η_{oo} ≈ 71%, pump efficiency η_p ≈ 63% at 200 K and for 4 kW/cm^2 to yield an effective conversion efficiency of η_{eff} ≈ 45%. Factoring in a median laser diode efficiency electrical to optical efficiency

of $\eta_o \approx 50\%$ a basic oscillator wall-plug efficiency of $\eta_{wp} \approx 22\%$ is projected. It is apparent that further efficiency optimization is possible with the various contributory factors to system wall plug efficiency, but η_{wp} = 25-30% is probably representative of a limiting condition. The free-space cavity length required, for filling factor modification to adjust pulse FWHM to desired duration, may be viewed as problematic in some applications. However, it may be reduced in physical dimension by integration into an engineered un-doped YAG mono-block for the free-space elements. Un-doped YAG has very low loss at 2 μm. Alternatively, the cavity can be folded.

Tm:YAG power amplifier

The pump dynamics of Tm:YAG have been presented. The challenge is efficient extraction. Again 200 K is favoured as an operating point. To attain the necessary intra gain medium fluence, without exposing optical elements to high fluences, a multi-pass arrangement is necessary. This should be configured so as to restrict transport losses, while constraining the cumulative surface fluence on the YAG medium to comfortably within the medium's LIDT for long pulse interactions. To minimise transport losses Brewster incidence optics and dielectric mirrors with adequate LIDT at 2 μm exist, and have limited reflectance differences between P and S polarizations at high reflection. Ideally, the mirrors should be retained structurally as far as possible in strictly P or S polarization reflection mode, although this may not be entirely possible within such a structure while maintaining the functionality desired. An assembly of two sequential mirrors is a possibility to appropriately configure the polarization of the beam for the remainder of its transit.

The possible multi-pass arrangement is similar to the oscillator configuration, with the exception that gain disc element and related structure is series scaled. Incident beams, at 20 J/cm^2, on gain media discs are at Brewster angles for low loss transport, and to eliminate need for AR coatings because the cumulative fluences of the overlaid beams in situ will be high. The majority of beam folding mirrors will be P polarized off normal reflection, as they will be in a common plane. For off normal reflection, surface fluence will be diminished. As in the oscillator schematic there will be one combination of two mirrors in series establishing a coupling to the additional beam transport plane wherein the subsequent structure will be a mirror image of the structure in the introductory plane. The two planes would each individually contribute a twofold overlay within the gain medium, resulting in a net four-fold overlay, of fluence enhancement. Alternatively, this can be viewed as a temporally overlaid four-way multi-pass, or even a sequential four-way multi-pass through the same gain medium. For the example presented, 14 folding mirrors are required, and as these mirrors present with reflectances of 99.7% and 99.9% for P and S polarizations respectively, the attributable transit loss will be less than ≈ 4%. This is tolerable for an amplifier. Pump access for bi-directional pumping of the disc elements is indicated by the cone structures and 45^o mirrors where required.

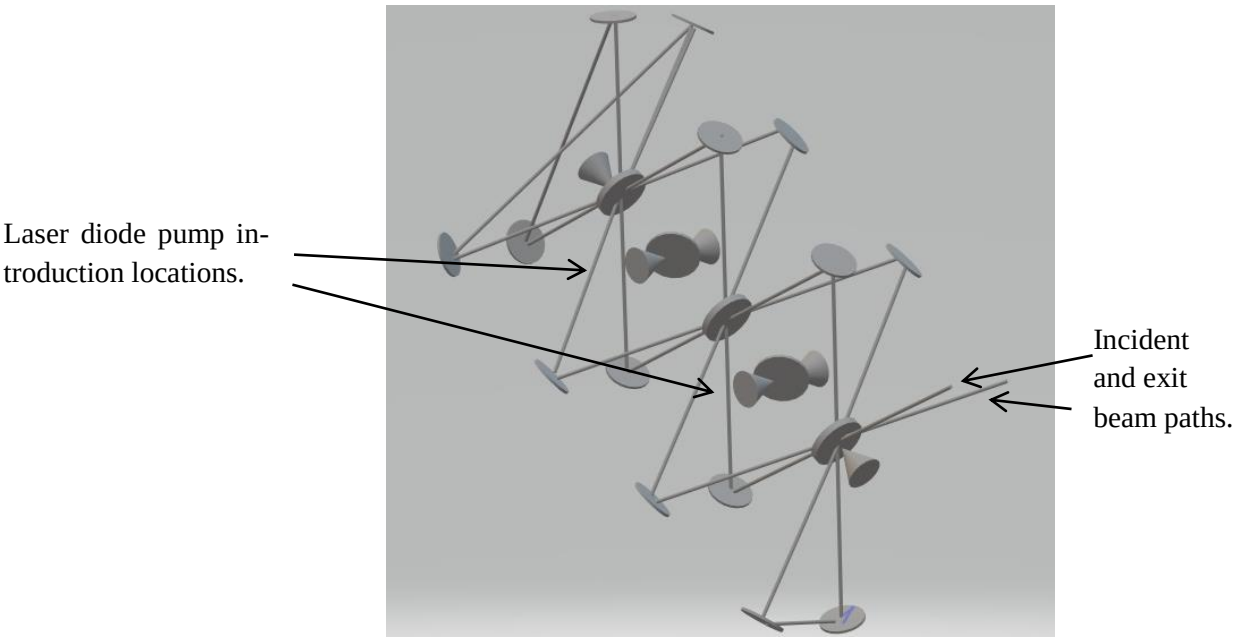

Figure 21. Pumping layout.

High fluence implies high efficiency. The extraction efficiency of a Tm:YAG amplifier, at 200 K, as a function of cumulative input fluence, is shown in Figure 22. Three cases have been considered: (i) Variation in extraction with on-axis incident fluence. (ii) Net extraction efficiency across the incident Gaussian profile, where the distribution peak corresponds to on-axis values, for a matched Gaussian pump distribution in the medium. (iii) Net extraction efficiency across an incident Gaussian distribution, for a matched top-hat pump distribution with a radial width of $\left(\frac{\pi}{2}\right) w_0$.

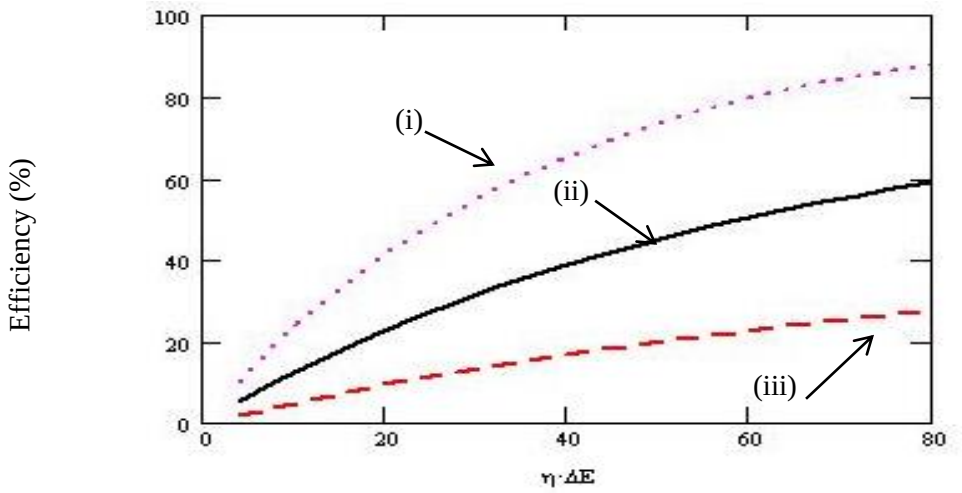

Figure 22. Extraction efficiency Tm:YAG at 200 K.

Case (ii) applies to a Gaussian output profile for a CO_2 PA pump. For a four beam folded arrangement the individual beam fluences are around 20 J/cm^2. This is within current optical element LIDT limits for long pulses of the duration under consideration here. If an in medium fluence of 80 J/cm^2 for long pulses is feasible, reasonable efficiency is attainable. From a bulk LIDT standpoint in YAG this is supportable. For a fluence at Brewster angle the corresponding surface LIDT is 70 J/cm^2. Utilizing typical scaling factors, such as $\sqrt{\frac{\tau}{\tau_{ref}}} \times \sqrt{\frac{\lambda}{\lambda_{ref}}}$, estimates of applicable LIDT are in the range 120-160 J/cm^2 [27-29, 36], where we have assumed a high standard of polishing, cleaning, and clean room assembly. The medium satisfies the condition that, for this specific system related pulsed duration space of interest, LIDT, bulk and effective surface, is significantly higher than the emission saturation fluence. For an operating amplifier the wall plug efficiency assuming 80 J/cm^2, is of the form $\delta \times \varphi \times \zeta$, or laser diode electrical to optical conversion efficiency×pump efficiency×extraction efficiency $\approx 0.5 \times 0.65 \times (100 \times 0.6) \approx 20\%$. The laser diode electrical to optical conversion approaches $\eta \approx 56\%$ at the pump wavelengths of interest, and with adequate pumping the pump efficiency can approach the theoretical limit of $\eta \approx 79\%$.

The oscillator and MOPA for the CO_2 pre-amplifier and power amplifier drive, could include free space anamorphic beam adjustment modification between oscillator and amplifier, or elsewhere, as required, to appropriately adjust the beam profile. The entire DPSS assembly would need to be enclosed in an inert dry gas environment.

This concludes the technical part of the report.

Estimate of the cost of a 5 to 10 TW 10 μm CO_2 USP laser operating at 10 Hz

Assumptions:

- *The cost estimate does not include labour costs.*
- *The major cost driver is the DPSS front end and related system components.*
- *A consistent extraction as required for the desired CO_2 pump.providing a competitive metric.*
- *A common oscillator out coupling is assumed.*
- *CO_2 preamp drivers, oscillators have a top hat irradiance profile.*
- *CO_2 power amp driver is a MOPA with a Gaussian output irradiance profile, this similarly requires an oscillator of Gaussian output irradiance profile*

The following provides the principle elements with performance estimates.

a) **CO_2 preamp drivers,** with active medium intracavity and ***double passed*** and low rep rate[(1)]. Drivers are oscillators. The combined net output required from these two units as a CO_2 pump is 30 J, of 100-200 ns FWHM. There is a requirement for two or more pump beams to facilitate

near axial uniformity of induced CO_2 pump. This may be generated by two or more, independent, but synced sources, or a single source that is appropriately split. This does not significantly modify the global cost.

	Room Temperature	**200 K**
LD array pricing (K$)	2×225 = 450	2×130 = 260
Medium gain length (cm)	2.9	1.9
Opt-Opt CE efficiency (%)	18	45
WPE (%)	9-11	21-26
LD PSU pricing (K$)	70	40
LD array cooling -10 Hz (K$)	10	6
Active medium cooling[(2)] (K$)	Readily available ≈ 10	Custom - ?

[(1)] LD arrays for pump pulse durations of interest are CW rated. Consequently, with appropriate engineering and enhanced thermal management, and some additional cost then, notably greater repetition rates are in principle achievable for the same installed LD array structures. In this case the corresponding repetition rate is 300 Hz relating to an average USP DPSS-CO_2 system power output of 1.5-3 kW. Power supply units are capable of sustaining the necessary average power, or switching at 10 Hz as considered here.

[(2)] Recommendation is cooling to 200 K. Gas, or liquid, or a combination are feasible.

→ Opt-Opt conversion efficiency incorporates isolated event pump efficiency factors, which are optimally for such events $\eta_p \approx 0.6$ at 200 K, and $\eta_p \approx 0.4$ at RT.
→ At higher rep rates it is anticipated to be better, or with given a more intense pump irradiance, but latter option may not be cost effective.
→ With limited parametrization modification in search of an optimal/limiting behaviour for this isolated pump event model, with cavity threshold determined by R_0, the oscillator Opt-Opt conversion efficiency limits around $\eta_{o\text{-}o} \approx 55\%$.
→ There is a notable reduction in requisite LD array costing for 200 K operation.
→ Independent cooling is required for the LD arrays and active medium.

CO_2 preamp driver *single passed*.

For low rep rate [(1)] and oscillator drivers, the net output required from these two units is ≈ 30 J. Two or more pump beams are required to ensure near axial uniformity of the CO_2 pump. This may be produced by two or more independent but synced sources, or splitting a single source. Selection of either approach does not modify the global cost.

	Room Temperature	200 K
LD array pricing (K$)	2×320 = 640	2×167 = 334
Medium gain length (cm)	4.2	2.5
Opt-Opt efficiency (%)	12	30
WPE (%)	6-7	15-18
LD PSU pricing (K$)	96	50
LD array cooling – 10Hz (K$)	15	7.5
Active medium cooling[(2)] (K$)	Readily available ≈ 15	Custom -?

[(1)] LD arrays for pump pulse durations of interest are CW rated. With appropriate engineering and enhanced thermal management, at an additional cost, greater repetition rates are in principle achievable for the same installed LD array structures. In this case the corresponding repetition rate is 300 Hz, which relates to an average DPSS-CO_2 system output of 1.5-3 kW. Power supply units are capable of sustaining the necessary average power, or switching at 10 Hz as considered here.

[(2)] Recommendation is cooling to 200 K using gas, or liquid, or a combination of.

→ Opt-Opt conversion efficiency at low rep rate incorporates isolated event pump efficiency factors, which are optimally $\eta_p \approx 0.6$ at 200 K, and $\eta_p \approx 0.4$ at RT.
→ Higher rep rates are anticipated to be better, but may not be cost effective if the methodology employed is to increase pump irradiance..
→ There is a clear reduction in the cost of LD arrays required at 200 K operation.
→ No parametric search has been undertaken for an optimal/limiting behaviour for a low rep rate single pass oscillator, as it is clearly not favourable compared with a double pass geometry.

b) **CO_2 power amp driver** - a MOPA arrangement. MOPA source is an oscillator as in part a). The associated DPSS PA is four way passed, at low rep rate [(1)]. Net output required from this system as a CO_2 pump is 100 J. This may be comprised of two or more reduced scale MOPAs, or a single device with appropriate beam splitting. Either approach does not modify the global

cost. Amplifier element assumes multi-pass at suitable fluences for the long pulse. A common attainable pumped inversion is assumed for cases.

	Room Temperature	**200 K**
LD array pricing (K$)	1400	960
Collective medium gain length (cm)	10	6
Opt-Opt CE (%)	26 (appropriate fluence, multi-pass)	40-45 (multi-pass, appropriate fluence)
WPE (%)	13 – 15.5	20 - 27
LD PSU pricing (K$)	210	140
LD array cooling: 10 Hz (K$)	30	20
Active medium cooling[(2)](K$)	Readily available ≈ 30	Custom - ?

[(1)] LD arrays for pump pulse durations of interest are CW rated. Consequently, with appropriate engineering and enhanced thermal management, and some additional cost, higher repetition rates are in principle achievable for the same installed LD array structures. In this case the repetition rate would be 300 Hz, corresponding to an average DPSS-CO_2 system output of 1.5-3 kW. Power supply units are capable of sustaining the necessary average power, or switching at 10 Hz, as considered here.

[(2)] Recommendation is cooling to ≈ 200 K using gas, liquid, or a combination of.

Additional system cost elements

→ Active medium – ballpark known – boules, of custom dopant level, will have to be custom grown/cut to dimension/optically finished as aperture wise the requirement is a bit larger than conventionally available ($30-50K).

→ LD array cooling units are approximately known – have to be able to handle average power factor of concern – with leeway to help with transient.

→ AOM/FTIR Q switch for device(s) plus driver.

→ Rest of optics as required, inclusive of diamond – miscellaneous manufacturing.

Conclusion for 10 Hz system, with further engineering to 100s Hz, LD array and related PSU costing

i. Function at 200 K, a modest temperature, is cost and performance-wise shown to be overwhelmingly indicated.

ii. Costing discrepancy between RT, for best case, and 200 K best case: RT system ≈ $2.26M and a 200 K system ≈ $1.46M, with a cooling method to be identified and implemented (gas, liquid, or a combination), with similar costs to RT case.

iii. Costing excludes labour, detail design and the engineering implementation.

iv. To make it more affordable a flashlamp pumped Cr:Tm:YAG system could be considered as a valid demonstrator, but it would not be scalable, regardless of engineering adaption, to increased repetition rates.

v. To conclude, the authors do not know what kind of mark-up would be applied in the industry for specialized, albeit 'production' systems. However, assuming 100%, and assuming manufacturing, optics and related aspects fall are less than $150K for a designed system, and assuming a 10 Hz system, the net costing would be ≈ 2×(1.46+0.15) ≈ $3.22M. Thermal management peripherals and associated gain medium engineering configuration for 300 Hz would increase the cost over that of a 10 Hz limited system. The resulting cost in dollars per Watt commercially would be $1000-2000 of average power, if scaled to 300 Hz. Given that a 10 Hz system has PSUs and LD arrays capable of sustaining 300 Hz, which are the primary system cost drivers, but are common to a 10 Hz device. This would be affordable for a unique research orientated system. Using indirect pumping it can be anticipated that system unit cost will decrease commensurate with the expected enhancement of optical to optical efficiency. The primary system cost driver is the LD array required. In this case the unit cost could halve approximately.

Bibliography

[1] J Ko *et al*., J. Phys. Chem. C, **120**, 3438 (2016)

[2] HS Kwak *et al.*, Disintegration of carbon dioxide molecules in a microwave plasma torch, Scientific reports, **5**, 18436 (2015)

[3] Siegmann (Lasers), pg129

[4] K.I Arshinov *et al.*, Collisional broadening of Vibrational-Rotational CO_2 lines by buffer gases, Atmospheric and Ocean Optics, (2020) **33**, 229

[5] JC Stephenson *et al*., J of Chem. Phys., **48**, 4790 (1968)

[6] C Krankel *et al*., Rare earth doped sesquioxides for diode pumped high power lasers in the 1- 2- and 3 μm spectral range, IEEE J of selected topics in Quantum electronics, **21**, 250 (2015)

[7] G Chen *et al*., Growth and spectra of Tm^{3+} doped $LuYO_3$ single crystal for 2 m lasers, Infrared physics and technology, https://doi.org/10.1016/j.infrared.2020.103431
[8] https://www.bnl.gov/atf/capabilities/co2laser.php
[9] S Marchetti *et al*., Accurate measurement of the refractive index of CO_2, N_2, He, O_2 and air at 10.57 µm at T=23C, Infrared physics & technology, **47**, 263 (2006)
[10] J. Zhang *et al*., Precision refractive index measurements of air, N_2 , O_2 , Ar and CO_2 with a frequency comb, Applied optics, **47**, 3143 (2008)
[11] LV Eckermann *et al*., Vibrational relaxation in CO_2 (10^00)-CO_2 collisions, ACS Earth Space Chem., **2**, 286 (2018)
[12] IV Pogorelsky *et al.*, The first picosecond terawatt CO_2 laser at the Brookhaven accelerator test facility, BNL-65240, (1998)
[13] IV Pogorelsky *et al*., BESTIA – the next generation ultra fast CO_2 laser for advanced accelerator research. BNL-111612-2015-JA, (2015)
[14] G Fibich *et al*., Self focusing of circularly polarized beams, Phys. Rev. E, **036622**, (2003)
[15] A Borzsonyi *et al*., Measurement of pressure dependent nonlinear refractive index of inert gases, Optics Express, **18**, 25847 (2010)
[16] C Bree *et al*., Method for computing the nonlinear refractive index via Keldysh theory, IEEE J of Quant. Electronics, **46**, 433 (2010)
[17] MN Polyanskiy *et al.*, Single shot measurement of non linear refractive index of air at 9.2 µm with a picosecond terawatt CO2 laser, Optics Letters, 10.1364/ol.423800, (2021)
[18] E Mareev *et al.*, Anomalous behaviour of nonlinear refractive indexes of CO2 and Xe in supercritical states, Optics Express, **26**, 13229 (2018)
[19] D Tovey *et al.*, Gain dynamics in a CO_2 active medium optically pumped at 4.3µm, J of Appl. Phys., **128**, 103103 (2020)
[20] RC Auyeung *et al*., IEEE J of Quantum Electronics, High vibrational temperatures in optically pumped CO_2, **24**, 753 (1988)
[21] T Sugawara *et al*., Instability in a CO_2 sequence band laser with a saturable absorber and vibration to vibration energy transfer process, J. Opt. Soc. Am. B, **10**, 265 (1993)
[22] S Doraiswamy *et al*., Vibrational modeling of CO_2 in high enthalpy nozzles flows, J. of Thermophysics and heat transfer, **24**, 9 (2010)
[23] S Reilly *et al.*, Laser induced damage threshold of CVD grown single crystal diamond surfaces with various surface finishes, Advanced solid state lasers conference, ATu2A.6.pdf (2015)
[24] P Borner, Ultra short pulse laser ablation of diamond, Thesis DISS. ETH No. 25846, (2019)
[25] SPAWR inc, Copper mirror damage threshold > $2.5 * 10^5 \sqrt{\tau_p} J/cm^2$
[26] NK Sherman *et al.*, Transient response of metals to ultrashort pulse excitation, Optical engineering, **28**, 1114 (1989)

[27] DE Zelmon *et al.,* Optical properties of Nd-doped ceramic yttrium aluminum garnet, proc of SPIE **5647**, 255 (2004)

[28] MJM Rodrigo *et al.,* Laser induced damage threshold of Yb:YAG crystals at stretched 150-ps pulses, Proc of SPIE **10513** (2018)

[29] JF Bisson *et al.*, Laser damage threshold of ceramic YAG, Jpn J Appl. Phys., **42**, L1025 (2003)

[30] J Korner *et al.,* Spectroscopic investigations of thulium doped YAG and YAP crystals between 77 K and 300 K for short wavelength infrared lasers; Journal of Luminescence, **202**, 427 (2018)

[31] TY Fan *et al*., Cryogenic Yb^{3+} doped solid state lasers, IEEE J of Selected topics in Quantum electronics; **13**, 448 (2007)

[32] JI Mackenzie *et al*., Modeling of high power continuous wave Tm:YAG side pumped double clad waveguide lasers, IEEE J of Quantum Electronics, **38**, 222 (2002)

[33] LB Shaw *et al*., Measurement of up-conversion energy transfer probabilities in Ho:$Y_3Al_5O_{12}$ and Tm:$Y_3Al_5O_{12}$, Physical review B, **50**, 6609 (1994)

[34] C Wood *et al*., Laser damage testing for ion beam sputtered optical coatings at 2 μm and 3 μm, Proc of SPIE vol **8039**, (2011)

[35] Edmund Optics 2 μm line mirrors

[36] J Wallace *et al*., LIDT wavelength scaling rule of thumb shown to be inaccurate, Laser Focus World – in reality, the commonly employed root scaling was established to be a lower bound (2015)

Accomplishments

Title of project

A conceptual and technical design study of an ultra-short pulse CO_2 laser driven laser wakefield accelerator, as a first step to developing a robust demonstrator

Original Abstract

The proposal is to produce a technical design of an optically pumped CO_2 laser driven laser wakefield accelerator. This will be undertaken using numerical and theoretical methods. Two strands of development will be undertaken simultaneously by a team of experts in CO_2 lasers and laser-plasma accelerators and radiation sources. The project will be undertaken over 24 months and two staff members will be employed at an FTE of 0.4 to ensure that the project staff can maintain links with existing programmes and also benefit from interaction with their colleagues. The main deliverables will be a fully costed technical design, component procurement, staffing and timeline for manufacturing a demonstrator that is suitable for a second stage where it would be constructed and demonstrated. A document evaluating potential applications will also be produced in consultation with the funder.

- *Research Objectives: Please list the main research objectives of this project*

List the major goals of the project including the scientific or technological objectives of this effort. Describe the proposed technical approach to obtain those goals. If the application listed milestones/target dates for important activities or phases of the project, identify these dates and show actual completion dates or the percentage of completion.

Original Objectives

Undertake a technical design study to establish a detail design of a CO_2 laser suitable for driving a LWFA and the LWFA.

1) Establish what performance characteristics would conform to a minimal, yet effective, demonstrator for 10 μm USP driver of a LWFA at a rep rate suitable for the contractor.
2) Double that, at least in pulsed energy, and therefore pulsed power, as a design objective.
3) Undertake general system simulations to establish a system configuration suitable for attaining the design objective output.
   a) More directly this most likely means assuming a primary OPA source and then establishing the unitary preamp specification required, followed by establishment of the most beneficial power amp configuration required. This exploiting the gain capability of the DPSS-CO_2 technology.
4) Given the roadmap established by the forgoing:
   a) DPSS front end
      i) Execute a system design for the preamp DPSS front end.
      ii) Execute preliminary engineering design of said unit.
      iii) Establish peripheral systems requirements.
      iv) Establishing sourcing and costing for entirety.

b) CO_2 preamplifier
   i) Execute system design for associated CO_2 component of preamp.
   ii) Execute preliminary engineering design of said unit.
   iii) Establish peripheral systems requirements.
   iv) Establish sourcing and costing for entirety.
c) DPSS power amp pump
   i) Execute system design for power amp DPSS front end.
   ii) Execute preliminary engineering design of said unit.
   iii) Establish peripheral systems requirements.
   iv) Establish sourcing and costing of entirety.
d) CO_2 power amplifier
   i) Execute system design for associated CO_2 component of power amp.
   ii) Execute preliminary engineering design of said unit.
   iii) Establish peripheral systems requirements.
   iv) Establish sourcing and costing of entirety.
e) LWFA design
   i) Undertake a design of a LWFA driven by a CO_2 USP laser, including the parameter range possible (charge, maximum energy, energy spread, emittance, bunch duration, stability etc.) using the CO_2 pump laser
   ii) Design the plasma medium (laser ionised gas jet, gas cell or preformed capillary plasma – to be determined)
   iii) Design an optical delivery system (lenses, mirrors) for delivering the CO_2 laser beam to the plasma
   iv) Design a diagnostic system to establish the LWFA characteristics
f) Design of vacuum chamber and radiation shield for the LWFA
g) Propose applications

- *Please provide details of accomplishments during this reporting period.*
    - *For this reporting period describe: 1) major activities; 2) specific objectives; 3) significant results or key outcomes, including major findings, developments, or conclusions (both positive and negative); and/or 4) other achievements. Include a discussion of stated goals not met.*

Accomplishments

Major activities and specific objectives

Three major activates were undertaken for the project: i) design of a laser wakefield accelerator (LWFA) based on a CO_2 laser, ii) design of an optically pumped CO_2 ultra-short pulsed laser based on direct and indirect pumping, and iii) determine the cost of building an optically pumped CO_2 laser prototype and a potential commercial device. This is described in a detailed report that is submitted as part of the overall report. The design studies of the LWFA and optically pumped CO_2 laser were undertaken in parallel. The CO_2 laser driven LWFA design studies were carried out at the University of Strathclyde, benefitting from an ongoing research programme to develop Ti:sapphire-pumped LWFAs and radiation sources at the University. The

design study of the optically pumped CO_2 laser was undertaken by IRP Technology LLC, Corrales, NM, USA as a sub-contract. The main people involved in the project were Prof. Dino Jaroszynski and Dr. Enrico Brunetti from Strathclyde, and Dr. Neil Campbell and Mr. Jack Lovell from IRP. Many other people from Strathclyde contributed to the work both directly and indirectly.

Significant results and key outcomes

LWFA design study

A comprehensive design of a LWFA pumped by a sub-picosecond pulsed CO_2 laser with energies ranging from 1- 400 J.

We performed particle-in-cell (PIC) simulations to model the interaction of an intense sub-picosecond laser pulse with wavelength of 10.6 μm and pre-ionised uniform plasma of varying length. We investigated a wide range of laser pulse durations, waist sizes and energies, corresponding to peak powers of 10s–100s TW. We used a pre-ionised uniform plasma with density of 10^{16}–10^{17} cm^{-3} and no external guiding, obtaining electron beams with energy up to 2 GeV and charge up to 100s nC, which is three orders of magnitude higher than what is achievable using near-infrared lasers of similar power. The laser-to-electron-beam conversion efficiency can exceed 50%.

- For example, a 20 TW CO_2 laser emitting pulses with 500 fs duration and 10 J energy focused to a waist size of 50 μm into a plasma with density of 1×10^{17} cm^{-3} and length of 16 mm produces an electron beam with mean energy of 230 MeV with 4% energy spread, 4 nC charge and 14 mrad r.m.s. divergence, selecting only the high-energy peak. The electron bunch energy is ≈ 1 J, which give a conversion efficiency of 10%, for this case.
- If the laser energy is increased to 100 J (P = 200 TW), the spot size to w_0 = 100 μm, and the plasma length is set to 20 mm, the mean energy of the selection is 560 MeV with 7% energy spread, 50 nC charge and 15 mrad r.m.s. divergence. If the laser energy is further increased to 400 J (P = 800 TW), with w_0 = 200 μm, $n_e = 2.5 \times 10^{16}$ cm^{-3} and a plasma length of 86 mm, the mean energy of the selection is 1.6 GeV with 12% energy spread, 140 nC charge and 6 mrad r.m.s. divergence. The electron bunch energy is 224 J, which results in a conversion efficiency of ≈ 56%.
- Such charge levels are significantly higher than what is expected from near-infrared lasers of similar power, although the bunch length and emittance can be larger. Nevertheless, currents of 100s kA are achievable. These results have been obtained in a pre-ionised plasma, but simulations performed using neutral helium indicate that a CO_2 laser can fully ionise the gas. Alternative schemes, such as plasma discharge waveguides or heater pulses can also be considered, especially for low laser powers. Here no attempt has been made to optimise parameters such as emittance, energy spread and bunch duration, but techniques such as down-ramp injection and density modulation could be used to control injection and the properties of the beam. Moreover, techniques based on ionisation injection could further boost the beam charge and conversion efficiency.

We have shown that a wide range of laser waist sizes and pulse durations can be employed, but the electron beam energy is maximised when $w_0 \approx \lambda_p$ and $T_{FWHM} \approx \lambda_p/2$, where λ_p is the plasma wavelength. The charge, on the other hand, is typically maximised for slightly smaller waist

sizes and longer pulse durations. However, self-guiding is often less effective for waist sizes smaller than 50 μm and pulse durations shorter than 250 fs, resulting in lower electron beam energies and charges, especially for low plasma densities and low laser energies. Under these conditions, external guiding can significantly enhance the electron beam energy. On the other hand, pulse durations approaching 1 ps can degrade the electron beam quality due to interaction with the laser field, but could potentially boost the emission of betatron radiation.

With advances in CO_2 laser technology, as proposed in the optically pumped CO_2 laser design study, LWFAs driven by these lasers could be ideal for applications that require high-charge electron beams, such as industrial imaging, activation analysis, radioisotope production and radiotherapy. A bright tuneable X-ray source could also be realised using Compton back-scattering. An optically pumped CO_2 laser driven LWFA would be efficient, compact, robust and could be made mobile.

Optically pumped CO2 laser

The basic conceptual design proposed and parametrized is a diode pumped solid state (DPSS) optically pumped ultra-short pulse (USP) CO_2 laser technology. This has potential to enable extreme light research and many other applications, including the LWFA. Two distinct CO_2 pump path options accessible to the identified DPSS front ends have been explored. The former as a proof of principle empirical investigation, the latter at this stage, theoretically. The first is direct pumping of the CO_2 transition(s), or a combination of transitions of a multi-isotopologue gas mix. The second is an indirect pump path incorporating a resonant transfer from a donor to an acceptor (i.e. CO_2).

The proposed system is broken down into a multi-pass pre-amplifier followed by one or more power amplifiers. Both chirped pulse amplification for USP amplification is considered in addition to the possibility of direct amplification of an USP in the amplifying medium.

A detailed design study has been undertaken, supported by simulations and analytic evaluation of the CO_2 amplifying medium under a range of gas pressures, compositions and system geometry, pumped using both direct and indirect pumping schemes. The constraints of non-linear focussing in optical components and the CO_2 gas were also a priori evaluated and apparent boundaries established for safe operation, which set constraints on a feasible pumping geometry of the multi-pass amplifiers. The viability of the design was established and comparison was made between ongoing experimental work not funded by this grant.

A design of an optical pump front end, as integral to the DPSS-CO_2 system is based on diode pumped Tm:YAG as a medium, as it has a number of favourable features, not least a suitable spectrum and long-excited level lifetime, which is particularly suited to pumping by affordable diode arrays. The dopant Thulium has a smaller emission cross section than Holmium, and, correspondingly, a larger saturation energy for pulsed operation. The application presented here is aimed at relatively long duration output pulses of 100 to 200ns, that are kinetically suited to Tm:YAG, which in turn are suited to pumping CO_2, moreover it mitigates a saturation energy issue by raising the laser-induced damage thresholds (LIDT). The energy storage of Tm:YAG is good and it has an acceptable gain-length product corresponding to useful gain lengths without risking amplification of spontaneous emission (ASE) or parasitic oscillation. It benefits from modest cooling and equally operates at cryogenic liquid N_2 temperatures. The host medium YAG has good thermal conductivity, thermo-optic and thermal expansion properties when cooled.

A preliminary estimate of the cost of a 10 Hz system (extendable to 100s Hz) has been evaluated for a range of active medium temperatures.

System operation at ~200 K is predicted to be optimal for a variety of reasons, including cost. Comparatively cost of a room temperature (RT) system was shown to be ≈$2.26M, yet a 200 K system is $1.46M, with a cooling method to be identified and implemented (gas, liquid, or a combination), with similar costs to the RT case as that is not the primary cost driver. These costs, however, exclude labour, detail design and the engineering implementation. It also excludes typical commercial mark-up. Assuming a commercial source and 100% mark-up, plus manufacturing, optics and related costs of less than $150K for a 10 Hz system at 200K, the net cost of a prototype are estimated to be ≈$3.22M.

We also suggest a more affordable flashlamp pumped Cr:Tm:YAG system that could be developed as a demonstrator, but this is inherently not scalable to higher rep rates. It would be considerably more affordable than the DPSS-CO_2 route because the primary laser diode driver cost is set aside.

To return to the primary DPSS-CO_2 concept, given thermal management and gain media configured for 300 Hz, the system average output power would be in the range of 1.5-3 kW. The corresponding dollars per Watt metric would be $1000-2000/Watt. This would be affordable as a unique research orientated system. Using indirect pumping it is anticipated that the performance comparable system unit cost will decrease commensurate with the expected enhancement of optical-to-optical efficiency.

Given that the primary system cost driver is the laser diode array required, the unit cost could halve approximately.

Dissemination

The outcome of the project has been disseminated using several channels, including workshops, conferences and publications. The publications are reported here. However, as we are applying for a patent to protect the IP generated by the project, the final major publication on the CO_2-driven LWFA will only be published in around 6 months in one of the Nature family journals, which will enable the patent to be filed.

The main target communities for dissemination are developers of the LWFA, because our project introduces a unique angle to the community: a CO2-driven LWFA produces considerably higher charge than a near infrared (800 nm) laser driven LWFA, it has much higher efficacy and is much more compact.

The main conferences where the results have been discussed are the SPIE Optics + Optoelectronics conference in Prague in 2021.

Impacts

The main impact of the project will be realised when a prototype system has been constructed, which will depend on future funding. We are planning to secure follow-on funding in the near future. The SCAPA facilities at Strathclyde provide an ideal laboratory environment for producing a prototype because of the availability of shielded bunkers for the LWFA and diagnostic equipment for evaluating a LWFA prototype and demonstrating it to potential commercial funders for the future commercialisation of the systems.

Development of the principal discipline(s) of the project

The design study undertaken as part of this project is a large step towards the realisation of a new generation of LWFAs with stable and compact laser drivers that could advance the technology to the point that it becomes reliable, stable and affordable. Moreover, because of the potentially higher repetition rate efficient optically pumped CO_2 lasers, as proposed in our design study, it could potentially replace some synchrotron sources with devices that could be housed in a university laboratory or within the confines or a company site. This would alleviate the bottlenecks in obtaining beam time at light sources, while also allow companies to maintain their IP confidentiality. Furthermore, when more users use the high efficiency optically-pumped CO_2 laser driven LWFA and light sources based on them, new uses will be found. The availability of affordable sources will encourage users to explore more uses of light sources.

With advances in CO_2 laser technology, as proposed in the optically pumped CO_2 laser design study, LWFAs driven by these lasers could be ideal for applications that require high-charge electron beams, such as industrial imaging, activation analysis, radioisotope production and radiotherapy. A bright tuneable X-ray source could also be realised using Compton back-scattering or compact undulators. An optically pumped CO_2 laser driven LWFA would be efficient, compact, robust and could be made mobile.

Other disciplines:

A wide range of users use light sources and electron beams. These include users of synchrotrons, clinicians using beams for radiotherapy and imaging, industrialist using beams for processing materials and sterilisation, numerous military applications and also the nuclear industry who require probing x-rays to image dense material for the stewardship of stored nuclear waste and for decommissioning of nuclear plants. Also, there is potential to use efficient XUV sources based on an optically pumped CO_2 driven LWFA for photolithography for chip manufacture for large scale electronics and detectors.

Describe the impact in this reporting period on the development of human resources

The project has provided an ideal opportunity for training scientists. In particular, a post-doctoral researcher at Strathclyde has been able to develop his skills on numerical simulation of LWFAs to the point where has become a world expert on LWFAs in the CO_2 wavelength range. The teams at IRP Technologies have been exposed to leading edge LWFA physics. Similarly, the Strathclyde team has been exposed to CO_2 laser technology development. The two teams have developed a unique partnership that places them in an ideal position to develop the combined technology further. The next step in the development is to produce a prototype and demonstrate its feasibility and realise a road map to its eventual commercialisation.

Describe the impact on teaching and educational experiences

The project has been a good opportunity in developing ways of disseminating the new technology opportunities.

Describe the impact in this reporting period on physical, institutional, and information resources that form infrastructure.

We have utilised the computational resources at Strathclyde and purchased a GPU computer system for particle-in-cell modelling of the LWFA. We have also benefitted from the ongoing

research in developing an 800 nm LWFA and radiation source at Strathclyde. Most of the LWFA research at Strathclyde can be re-evaluated at 10 μm using CO_2 laser technology. This will allow excellent comparative studies to be undertaken, which will speed up future developments.

Impact on society beyond science and technology:

If the optically pumped CO_2 laser driven LWFA technology can be made more widely available at low cost, it would have a profound effect on the use of light sources and high energy beams.

The very significant cost reduction offered by the CO_2 driven LWFA of this proposal, and its turnkey nature, open the door to broad academic and industrial use, and make the solution widely deployable even to 3rd world countries. Apart from a multitude of roles in the academic sphere, our customer discovery efforts have identified more than thirty applications across ten industries that this combined technology either makes commercially viable for the first time or to which it will bring eagerly sought-after performance and operational improvements.

Changes

No changes have been made. All the goals have been met. The eventual realisation of a demonstrator would benefit from the resident expertise in radiation shielding, beam transport and safety, which would be evaluated for developing a prototype. SCAPA is a world-leading facility that provides laser beams to academic and industrial users.

Changes in approach

No significant changes were made.

Problems or delays

No delays.

Expenditure Impacts

No expenditure impact.

Technical Updates

The attached technical report presents a comprehensive and detailed description of the design study and an estimate of the eventual costs of a system.